Ph.D. Dissertation of Min Jung Kim

Cell Free Supernatants of Bifidobacterium: *B. adolescentis* and *B. longum* Suppress Cancer Growth in a Colorectal Cancer Organoid Model

August 2023

Graduate School of Medicine
Seoul National University
Surgery Major

Min Jung Kim

Cell Free Supernatants of Bifidobacterium: *B. adolescentis* and *B. longum* Suppress the Growth in Colorectal Cancer Organoid Model

Submitting a Ph.D. Dissertation of
Public Administration
June 2023

Graduate School of Medicine
Seoul National University
Surgery Major
Min Jung Kim

Confirming the Ph.D. Dissertation written by
Min Jung Kim
June 2023

Chair _____(Seal)
Vice Chair _____(Seal)
Examiner _____(Seal)
Examiner _____(Seal)
Examiner _____(Seal)

Abstract

The gut microbiome and its metabolites are pivotal in regulating host metabolism, inflammation, and immunity. Host genetics, colonization at birth, host lifestyle, and exposure to diseases and drugs determine microbial composition. Dysbiosis and disruption of homeostasis in the microbiome have been reported to be involved in the tumorigenesis and progression of colorectal cancer (CRC). However, the role of metabolites secreted by the bacteria in the growth of CRC is still unclear. Here, we compared the microbial composition of CRC patients with healthy controls to identify distinct patterns of microbiota-derived metabolites in CRC. The metagenomic analysis demonstrated that *Blautia producta*, *Bifidobacterium adolescentis*, and *Bifidobacterium longum* decreased, while *Parabacteroides distasonis* and *Bacteroides ovatus* were more prevalent in the CRC patient group. Cancer organoid lines were treated with the microbial culture supernatants of these five strains, resulting in considerable cancer growth inhibition and apoptotic effects by *Bifidobacterium* supernatants. This study demonstrates that the bacterial metabolites depleted in CRC patients may inhibit cancer growth and highlights the effects of microbiome-derived metabolites on CRC growth.

Keywords : colorectal cancer, microbiome, Bifidobacterium, organoid, metabolite
Student Number : 2014-30616

Table of Contents

Chapter 1. Introduction

1.1. Study Background

Colorectal cancer (CRC) is the third most diagnosed cancer worldwide, accounting for 10% of all new cancer cases annually (Dekker, Tanis, Vleugels, Kasi, & Wallace, 2019; Siegel, Miller, Wagle, & Jemal, 2023). Of all cancer-related deaths, 9% of men and 8% of women died due to CRC. In South Korea, CRC is also the third most diagnosed cancer, with 27 877 new cases reported in 2020, and 8869 deaths attributed to CRC (Kang et al., 2023). The number of prevalent CRC cases in Korea was 292 586 in 2020.

Although the incidence of CRC has decreased due to nationwide screening programs and increased adoption of colonoscopy, the number of patients younger than 50 years presenting with CRC has been steadily increasing in high-income countries since 1988, especially for left-sided CRC and rectal cancer (Sinicrope, 2022).

The development of CRC is influenced by both environmental and hereditary risk factors (Dekker et al., 2019). With varied risks depending on the age of CRC diagnosis and the number and degree of affected relatives, approximately 10–20% of CRC patients have a positive family history. Environmental risk factors include smoking, alcohol intake, red and processed meat consumption, and increased body weight. Notably, certain microbial species in the colon, such as *Fusobacterium nucleatum* and *Bacteroides fragilis*, may increase the risk of CRC incidence (Kostic et al., 2013; Nakatsu et al., 2015). Most cases of early-onset CRC are sporadic attributed to multiple risk factors, including a Western-style diet that can lead to gut dysbiosis, chronic inflammation, and ultimately CRC tumorigenesis (Mehta et al., 2017; Sinicrope, 2022).

The gut microbiome is the closest micro-environment to the colon epithelium, and it reflects the host's lifestyle and external environments since birth (Yatsunenko et al., 2012). Researchers have found that the microbial composition of patients with CRC differs from that of healthy controls. They suggest that an abundance or

depletion of the gut microbiome might play a role in CRC tumorigenesis or progression (Feng et al., 2015; Flemer et al., 2017; Nakatsu et al., 2015; Vogtmann et al., 2016; Zeller et al., 2014). According to a meta-analysis study across eight metagenomics studies, the CRC metagenome had a core set of 29 species that were considerably abundant. These species included *Fusobacterium*, *Porphyromonas*, *Parvimonas*, *Peptostreptococcus*, *Gemella*, *Prevotella*, and *Solobacteriulm* (Wirbel et al., 2019).

Although the gut microbiome's role in the initiation and progression of CRC has been extensively studied, the entire map has not yet been completed. Certain bacterial species, such as *Fusobacterium nucleatum*, *Peptostreptococcus anaerobius*, and enterotoxigenic *Bacterodes fragilis,* have been reported to contribute to CRC carcinogenesis by accelerating tumor growth (Y. Yang et al., 2017), causing DNA damage (Rubinstein et al., 2013), enhancing inflammation (Chung et al., 2018), and helping immune evasion of tumors (Long et al., 2019). Conversely, some species such as, Lactobacillus and Bifidobacterium are depleted in CRC patients, which may have a protective effect against CRC by regulating colonic inflammation (Khazaie et al., 2012; Mohamadzadeh et al., 2011).

The microbiome generates its metabolome in the colonic lumen, and a small portion of it is absorbed through the colonic mucosa and enters the blood stream (Louis, Hold, & Flint, 2014). A tumorigenic or anti-tumorigenic signal to CRC may be elicited by the metabolome, which is the net metabolic output of the entire gut microbiome rather than the product of a single microorganism. The major fermentation products are gases and organic acids, including short-chain fatty acids (SCFAs), particularly butyrate, acetate, and propionate.

SCFAs, phenolic acids, and isothiocyanates are known for their anti-carcinogenic properties. The proposed underlying mechanism involves G protein-coupled receptor mediated signaling that promotes the differentiation of regulatory T cells and IL-10-producing T cells, blocks activation of nuclear factor-kB (NF-kB), and induces apoptosis through histone deacetylase inhibition (Brown et al., 2003; Maslowski et al., 2009; Singh et al., 2014; Thangaraju et al., 2009). On the other hand, microbial fermentation products from proteins, including polyamines, hydrogen sulfide, and secondary bile

acids, have pro-carcinogenic properties.

However, it is still unclear how the metabolome of specific species, which differs in the gut of CRC patients compared to healthy controls, affects CRC growth.

1.2. Purpose of Research

This research aimed to identify the microorganisms that were depleted or enriched in the colon of CRC patients and to test the effect of the microorganisms' metabolome on CRC growth *in vitro* using CRC and colon epithelial organoids.

Chapter 2. Body

2.1. Materials and Methods

2.1.1. Collection of fecal samples

The fecal samples from CRC patients and healthy controls were collected and analyzed. The fecal samples from CRC patients were collected at the National Cancer Center, Goyang, between June 2002, and April 2004. The stools from healthy controls were collected at the health check-up center in Seoul National University Hospital, Seoul, and selected through age and sex-matched selection. Participants collected the stool samples in a tube, submitted them to the institution, and they were frozen and stored at -20 °C.
Prior to obtaining samples, we obtained the patient's informed consent for their use in this study. The institutional review board of Seoul National University Hospital approved this study (IRB no. 1701-110-826).

2.1.2. 16S bacterial rRNA analysis

Whole DNA in fecal samples was extracted using the Mag-Bind Universal Pathogen 96 Kit (Omega Bio-Tek, Norcross, GA, USA) with a Hamilton Microlab STAR liquid handler (Hamilton Laboratory Solutions, Manitowoc, WI, USA) after bead-beating the samples with the TissueLyser (Qiagen, Hilden, Germany), followed by amplicon PCR targeting the V3 to V4 region of the 16S bacterial rRNA gene using 341F and 805R primers (341F-CCTACGGGNGGCWGCAG, 805R-GACTACHVGGGTATCTAATCC). After DNA library preparation, indexing and quality checks were performed using the Nextera XT index kit (Illumina, San Diego, CA, USA) and Qubit4.0 (Thermofisher, Wilmington, DE, USA), and 300 × 2 paired-end sequencing was performed using the MiSeq system (Illumina, San Diego, CA, USA). The raw FASTQ files had an average read depth of more than 50,000 counts. A pre-trained classifier using Silva138 classified the denoised amplicon sequence variant (ASV) features acquired after DADA2 in QIIME2 2020.2 (qiime dada2).(Bokulich et

al., 2018; Bolyen et al., 2019; Callahan et al., 2016; Quast et al., 2013).

2.1.3. Sample preparations of CRC and colon epithelium for organoid culture

Tissue samples from CRC patients obtained from surgical specimens were transported immediately to the laboratory in a fresh state. Tissue biopsies were mechanically dissociated using surgical scissors and digested using an enzyme solution containing collagenase II (1.5 mg/mL, Gibco, 17101-015-1G), hyaluronidase (20 μg/mL, Sigma Aldrich, H3506-100 MG), and Y-27632 (10 μM, Sigma Aldrich, Y0503-5 MG) in DME/F12 medium (supplemented with penicillin and streptomycin). The tissue was incubated at 37 ° C with gentle rotation for 1 h, after which the pellets were collected by filtering through a 100 μm-pore cell strainer. The pellets were then resuspended in RGF-BME matrigel and seeded onto 24-well plates. The isolated cancer epithelium (tumor) and crypts (normal) were fed with human intestinal stem cell (HISC) medium supplemented with 10 μM Y-27632 for the first 3 days of culture to prevent anoikis.

2.1.4. Organoid culture medium

To produce a complete organoid culture medium, a conditioned medium and a basal culture medium were mixed in a 1:1 ratio and supplemented with various growth factors, including B27 (1X, Gibco, 17504-044-50X, 10 mL), n-acetyl cysteine (1.25 mM, Sigma Aldrich, A7250-5G), nicotinamide (10 mM, Sigma Aldrich, 72340-100 G), hEGF (0.1 mg/mL, Thermo Fisher Scientific, PHG0311L-0.1 mg), hFGF10 (10 ng/mL, Thermo Fisher Scientific, PHG0204-25 μg), A83-01 (500 nM, Sigma Aldrich, SML0788-5MG), SB202190 (3 μM, Sigma Aldrich, S7067-5MG), Prostaglandin E2 (10 nM, Sigma Aldrich, P5640-1MG), and contamination-blocking antibiotics (Primocin, 100 μg/mL, Thermo Fisher Scientific, ant-pm-1–10*1 mL 500 mg). The conditioned medium was prefabricated

in advance using a stably transfected cell line purchased from ATCC (L-WRN-transfected), which secreted Wnt-3a, R-spondin, and noggin proteins into the culture medium. Following the selection process for transfected-only cells, the cell line was thawed and cultured with DME/F-12 supplemented with 10% fetal bovine serum and 1% penicillin/streptomycin. The selection markers used were hygromycin B (500 μg/mL) and G418 (2.0 mg/mL). The basal culture medium was made up of GlutaMax (10 mM, Thermo Fisher Scientific, 35050-061 100 ML) and DME/F12, which was supplemented with 10% FBS and 1% penicillin and streptomycin.

2.1.5. Organoid culture

We established and cultured three sets of organoid lines (SNU-7237-TO, SNU-7293-TO, and SNU-7390S3-TO) derived from CRC patients, as well as their corresponding normal organoid lines (SNU-7237N-NO, SNU-7239N-NO, and SNU-7390N-NO) for this study. Tumor organoid lines were passaged using TrypLE express (Gibco, 12604), which was resuspended in DME/F12 supplemented with 5% BCS to dissociate organoids into single cells. The dissociated cell solution was centrifuged at 1500 rpm for 3 min, and the pellet was mixed with RGF-BME and seeded onto a new 6-well plate. Normal organoids were passaged using Cell Recovery Solution (Corning, 354253 100 mL). Organoid pellets that had been harvested and collected were gently resuspended with Cell Recovery Solution and incubated at 4 °C for 30 min to split them into single crypts. Matrigel was liquefied by mechanical pipetting (30–50 times), and the subsequent culture process was identical to that of the tumor organoid lines.

2.1.6. STR profiling

Genomic DNA was extracted from each organoid line using the AmpF1STR PCR amplification kit (Applied Biosystems, Foster City, CA). The amplified DNA was then analyzed using a genetic analyzer (Applied Biosystems 3500/3500xL Genetic Analyzer, Foster City,

CA) to detect minisatellites and decipher their short tandem repeat (STR) profiles. The STR marker library used for profiling included D8S1179, D21S11, D7S820, CSF1PO, D3S1358, TH01, D13S317, D16S539, D2S1338, D19S433, Vwa, TPOX, and D18S51.

2.1.7. **Treatment of cell-free microbial supernatant with organoids**

A hemocytometer was used to calculate the seeding concentration. A white 96-well opaque well plate (SPL, 30196) with 4000 cells per well was seeded, and differentiation and organoid formation were allowed to occur for 4 days. Each microbial cell-free supernatant was then diluted to a 25% concentration in HISC (organoid medium) medium. The cell-free supernatant was obtained from six strains: RCM (Normal culture medium, Reinforced clostridial medium), *Blautia producta* (KCTC 15607), *Parabacteroides distasonis* (KCTC 5751), *Bacteroides ovatus* (KCTC 5827), *Bifidobacterium adolescentis* (KCTC 3216), and *Bifidobacterium longum* (KCTC 3218). Additionally, the pH of all microbial cell-free supernatants was adjusted to $6.8 \leq pH \leq 7.2$ by adding 1.0 M NaOH and measured by a pH meter. The supernatants containing culture medium and organoids were co-cultured for 3 days.

2.1.8. **RLU measurement for Cell viability assay**

A 3D organoid culture model using CellTiter-Glo® 3D, which is used for evaluating cellular ATP levels, was used to assess viable cells and cytotoxicity. The reagent was thawed and equilibrated to room temperature before use, and all experimental procedures were performed at room temperature. The half volume of the culture solution (containing bacterial supernatant) was replaced with CellTiter-Glo® 3D (Promega, G9683) and thoroughly resuspended using a multi-channel pipette. Plates for screening were sealed with aluminum foil and incubated for 30 min. The luminescence of intra-organoid ATP content was quantified using Varioskan Lux (Thermo Fisher Scientific, USA) following the light-excluded incubation.

2.1.9. High-throughput Screening

We used the ImageXpress Micro Confocal 4 (Molecular Devices, USA) and corresponding image analysis software (MetaXpress, Molecular Devices, USA) to establish the HCS system. For screening, we selected the μ-Plate Angiogenesis 96-well (Ibidi, 89646, Germany) and calibrated it accordingly. Our previously reported method was partially applied to this study (Song et al., 2022). We seeded 4000 cells per well, derived from organoids, onto 10 μL of RGF-BME gel that had been previously dispensed and solidified in each well of the plate. The organoid medium included 4% RGF-BME as a feeding ingredient for the ECM on the side of the organoid that faced the culture medium. The seeded organoids were allowed to grow for 4 days and then treated with bacterial supernatant at a proportion of 25% culture in the medium. High-throughput screening was performed at 3-, 6-, and 12-days post-treatment using a 4x apochromatic objective lens, z-stacking, and z-projection.

2.1.10. **RNA sequencing**

Total RNA was isolated from cell lysate using TRIzol (Qiagen, Hilden, Germany) and the Qiagen RNeasy Kit (Qiagen, Hilden, Germany). Paired-end sequencing reads from cDNA libraries (101 bp) were generated with an Illumina NovaSeq6000 instrument, and the sequence quality was verified with FastQC v.0.11.7 (https://www.bioinformatics.babraham.ac.uk/projects/fastqc). For data preprocessing, Trimmomatic v 0.38 was used to trim low-quality bases and adapter sequences in reads (Bolger, Lohse, & Usadel, 2014). The trimmed reads were aligned to the human genome (UCSC hg19) using HISAT v2.1.0, a splice-aware aligner (D. Kim, Langmead, & Salzberg, 2015). Subsequently, transcripts including novel splice variants were assembled with StringTie v1.3.4d (Pertea et al., 2015). The abundance of these transcripts in each sample was calculated as read counts or TPM (Transcript per Million mapped reads) values. The dist and prcomp functions from the ggdendro (v0.1.22) and ggfortify (v0.4.11) R packages were used, respectively, to perform principal components analysis and validate

the similarity distance among the samples. To access the internal data of gene loading and analyze the contributing variables of PC2, which splits the samples by beneficial and harmful intestinal bacteria, the loading components were calculated by advanced features of the pca function from the PCAtools (v1.2.0) R package. The 20 highest loading components containing both positive and negative values in PC2 were plotted in a bar graph. The hosted MSigDB gene set database of the KEGG library (c2.cp.kegg.v7.4.symbols.gmt) was utilized by GSEA (v4.1.0) to perform single-sample enrichment-level analysis of cell signaling pathways based on the raw read counts of 35 993 transcripts. The phenotype label was designated as either normal colon mucosa versus tumor tissue or versus corresponding tumor derivatives for the normalized enrichment score (NES) of a single sample. The independent NES of a paired sample (normal and tumor) was calculated on default fields with a setting of permutations at 1000 and phenotype. The result was annotated by the NCBI Gene ID MsigDB.v7.4.chip platform. The total of overlapped pathways (50 gene sets of the KEGG pathway) that were significantly different (FDR < 0.25) compared to those of the healthy controls in both multiple tumors and PDOs (patient-derived organoids) were selected to identify the recapitulations of differentially expressed pathways in derived models. Using the ComplexHeatmap (v2.2.0) R package, heatmaps of NES values were plotted, and the mapped color variance was set between the minimum and maximum values.

2.1.11. Gas chromatography

Supernatants from the bacterial culture were harvested at $O.D_{600}$ values of 0.35–0.40. Methanol was added to the samples in a 1:1 ratio, and the resulting mixture was vortexed and sonicated for 10 min. After centrifugation at 13000 rpm and 4 ℃ for 10 min, the supernatant was collected and dried using a speed vacuum at 10 000 ppm (1 mg/mL). The dried sample was reconstituted in 150 μL of distilled water and then transferred to a new Eppendorf tube. The sample was dried again within a speed vacuum, and derivatization was performed. Gas chromatography was carried out using a GC-TOF-

MS (LECO Corporation, US) with a Rtx-5MS column and helium gas for analysis. The split ratio was set at 20:1, and three analytical replicates were performed.

2.2. Results

2.2.1. Schematic Diagram

The schematic diagram illustrates the overall flow of the study (Figure 1). To visualize the experimental design, we utilized a web-based graphic design platform with BioRender (https://biorender.com/).

2.2.2. Demographics

A total of 80 stool samples were collected, 40 from healthy controls and 40 from patients diagnosed with CRC at stages I–IV. The TNM classifications and AJCC stages are summarized in Figure 2A. The average age in the control group and the CRC group was 60.6±8.3 years (male-to-female ratio of 25:15) and 58.5±10.8 years (male-to-female ratio of 26:14), respectively. The most frequently distributed TNM classification was T3 (N=28, 70%), N0 (N=19, 47%), and M0 (N=29, 72.5%). Additionally, 92.5% of the patients were diagnosed with stage 2 or higher. Although the sex ratio of the donors was imbalanced (25:15), this did not affect the purpose of the study.

2.2.3. Metagenomic analysis

We first performed a diversity analysis to compare the beta diversity between healthy controls and CRC patients. The alpha diversity showed no difference between the two groups (Figure 2B); however, the two groups were distinctly separated and clustered in the beta diversity analysis (Figure 2C).

At the phylum level, phylum Firmicutes was more abundant in the healthy controls than in CRC patients and phylum Bacteroidetes was more abundant in CRC patients (Figure 2D).

To identify the differential features, we used LEfSe (Linear Discriminant Analysis Effect Size) to rank the strains. The 16 strains in the patient group and the 26 strains (including 3 undetermined strains) in the control group showed a noticeable distribution in each group by comparison of their means for statistical significance (Figure 2E). The differential strains were shown as a cladogram (Figure 2F). The species that were more abundant or depleted in CRC patients are listed in Table 1 and supplementary figures. Representatively, *Blautia obeum*, *Blautia producta*, *Faecalibacterium prausnitzii*, *Bifidobacterium longum*, *Bifidobacterium adolescentis*, and *Lactobacillus ruminis* were the more abundant species in the fecal samples of healthy controls. *Bacteroides ovatus*, *Parabacteroides distasonis*, *Bacteroides uniformis*, and *Parabacteroides gordonii* were the more abundant species in the fecal samples of CRC patients.

2.2.4. Establishment of colon normal and tumor organoid lines

To establish organoid cultures, we isolated crypts from normal tissue and the cancerous epithelium of tumor tissue, respectively. Each crypt was seeded in matrigel and passaged up to six times to establish organoid lines. We took great care to avoid bacterial or fungal contamination during the culture process. Organoid lines were maintained with periodic feeding and cautious subculture to optimize experimental conditions. Morphological differences were observed between CRC organoids (Figure 3A) and normal colon epithelium organoids (Figure 3B). Specifically, normal organoids exhibited branched crypts that were absent in tumor organoids. Each normal organoid line was passaged every 3–4 days, while tumor organoid lines were passaged every 10–14 days. We confirmed the identity of all organoid lines by matching their STR profiles with their parental tissue.

2.2.5. Addition of bacterial supernatants to organoid culture media

Cultured supernatants were harvested from five bacterial strains, namely *Blautia producta*, *Bifidobacterium adolescentis*, *Bifidobacterium longum*, *Parabacteroides distasonis*, and *Bacteroides*

ovatus. These supernatants containing the metabolome were then used to treat three CRC organoid lines (SNU-7237-TO, SNU-7293-TO, and SNU-7390S3-TO).

To perform the assay, 4000 dissociated cells were seeded onto a 96-well plate and incubated with the organoid culture medium mixed with each supernatant at a concentration of 20%. Morphological changes and cell viability assays were performed at three different time points (3-s, 6-, and 12-days) after the treatment. We observed a pattern of suppressed tumor growth and proliferation as early as 3 days after treatment, except in the case of the tumor organoids treated with *Bacteroides ovatus,* which was relatively enriched in the CRC fecal samples (Figure 4A, 4B).

Each conditioned medium containing bifidobacterial strains distinctly decreased the viability of the CRC organoids, as confirmed by RLU quantification (Figure 4C). In contrast, the addition of bifidobacterial supernatant to the organoid culture media did not affect the viability of normal colon epithelium organoids (Figure 4D).

Additional perimeter analysis was conducted using bright field images of organoids treated with bacterial culture supernatants. The median diameter of organoids was 644.85 μm, 666.1 μm, 659.86 μm, 663.86 μm, 562.33 μm, and 550.78 μm treated with HISC; RCM; and *B. producta*, *B. ovatus*, *B. adolescentis*, and *B. longum* supernatants, respectively (Figure 4E).

2.2.6. Transcriptomic impact of the bacterial metabolome

We analyzed transcriptomic profile alterations caused by different types of bacteria by exposing both normal and tumor organoids to bacterial culture media. Principle component analysis (PCA) separated bacteria enriched in normal tissue (Bifidobacterium longum and Bifidobacterium adolescentis) from bacteria enriched in cancer tissue (Bacteroides ovatus and Parabacteroides distasonis). We selected the top 20 differentially expressed genes between those groups (Figure 5A). CYP1A1, known as one of the cytochrome P450 enzymes, was highly upregulated by bacteria enriched in normal tissue and has been implicated in cancer prevention by detoxifying microenvironmental tumorigenesis factors [24]. In contrast, DKK4

(Dickkopf protein 4), which displayed a higher mRNA expression in bacteria enriched in cancer tissue, is known to be upregulated in CRC [25] and associated with the resistance mechanisms of 5-FU and YN968D1 in CRC cells [26]. We further investigated cancer pathways that were mostly affected by the bacterial metabolome by applying hallmark gene sets (Figure 5B). Bacteria culture media (Reinforced clostridial medium) was used as a mock control as it affects the transcriptomic patterns of both normal and tumor organoids. In general, the transcriptomic profiles of normal organoids were highly susceptible to bacterial culture media. Among tumor organoids, treatment with bacteria enriched in normal cancer downregulated angiogenesis as well as UV response pathways (highlighted with bold squares). Reactive oxygen species pathways were specifically upregulated by bacteria enriched in normal cancer (highlighted with bold squares).

2.2.7. Component analysis of bacterial culture supernatants

A component analysis was conducted to identify the composition of metabolites in bacterial cell-free supernatants, and the supernatant groups were divided into two categories: the cancer group (*Parabacteroides distasonis* and *Bacteroides ovatus*) and the normal group (*Bifidobacterium adolescentis* and *Bifidobacterium longum*). Each group was normalized by referring to the microbial culture medium (RCM).

Only gamma-aminobutyric acid (GABA) and cystine were prevalent in the cancer group compared to the normal group, whereas asparagine, tyrosine, and aspartic acid were observed in higher proportions in the normal group. (Figure 1A). Furthermore, to select metabolites showing relative disparities in content degree between normal and cancer patients, we sorted VIP (Variable Importance in Projection) values obtained from the OPLS-DA model based on values >1.0. The data were normalized with the mean of the total. To confirm the quantitative gap between the two groups, we performed the Mann–Whitney U test, and we notated an 'a' after the name of metabolites in a heatmap column when the p-value was below 0.05 (Figure 1A).

From the SCFA analysis of the supernatants (Figure 6B), we found that butyric acid was only detected in the bacterial supernatants of *Bifidobacterium adolescentis* and *Bifidobacterium longum*. Butyric acid is known for its beneficial function as a metabolic energy source for the colon epithelium (Louis & Flint, 2017) and as an HDAC inhibitor linked to the suppression of tumorigenesis in CRC (Fellows et al., 2018). Conversely, a higher concentration of acetic acid was observed in cancer patients, and the level of propionic acid was dramatically higher in *Parabacteroides distasonis* samples compared to those of other samples. A recent study reported that the level of isovaleric acid was higher in the SCFA profiles of CRC patients, supporting the idea that *Parabacteroides distasonis* and *Bacteroides ovatus* produce and secrete tumor metabolites through their physiological activity (Bosch, Berkhout, Ben Larbi, de Meij, & de Boer, 2019). Valeric acid was not detected in our samples.

We used the raw data from the GC-TOF-MS analysis to perform multivariate statistical analysis (Figure 6C). PCA allowed for the separation of healthy controls from cancer patients as well as the variations between healthy controls. In addition, we performed OPLS-DA to validate and enhance the differences between the participants.

2.3. Discussion

The intake of beneficial bacteria in the gut prevents CRC by improving the quantitative and qualitative composition of the gut microbiome (Chang, Shim, Cha, Reaney, & Chee, 2012; Zhang et al., 2015; Zhu et al., 2014). Extracts of *Bifidobacterium adolescentis* inhibit the growth of CRC cell lines by inhibiting β-glucuronidase, tryptophanase, and urease activity (Y. Kim et al., 2008). Additionally, intake of *Bifidobacterium longum* as a probiotic by CRC patients shifts the composition of the gut microbiome towards improved richness and diversity, resulting in increased tight junction integrity and decreased cell permeability, which play a critical role in preventing CRC (Liu et al., 2011). In our study, we verified the effectiveness of *Bifidobacterium* supernatant using the 3D CRC organoid model, which

is known to mimic improved physiological properties compared to 2D cell lines.

The microbiome has gained much attention in the last decade due to its roles in the development of several *in vivo* systems, including immunity, gut epithelium, and the brain (Arrieta, Stiemsma, Amenyogbe, Brown, & Finlay, 2014; Martinez, 2014; Olszak et al., 2012; Sommer & Backhed, 2013; I. Yang et al., 2016). Our data suggest that metabolites secreted from commensal bacteria play a pivotal role in the anti-cancer effects of cell death and growth arrest in CRC organoid models. One of the SCFAs, butyrate, is a major energy source for colonocytes and serves to maintain intestinal robustness through its anti-inflammatory function (Arrieta et al., 2014). Butyrate is produced in the gut by beneficial bacteria bearing genes coding for butyryl-CoA dehydrogenase, butyryl-CoA transferase, and butyrate kinase (Parada Venegas et al., 2019; Vital, Howe, & Tiedje, 2014).

Our study demonstrates that beneficial bacteria have an inhibitory effect on cancer not only in CRC cell lines but also in 3D organoid models, which are currently attracting attention as a substitute for mammalian models at the primary stage of drug development. In addition, with the development of genomic analysis technology, metagenomic and transcriptional analyses can be performed from the stools of healthy controls and actual clinical patients. The recent introduction of high-throughput screening systems as a screening platform for various biomedical research, enables the analysis and tracing of phenotypical changes after treatment with microbial supplements.

Chapter 3. Conclusions

The fecal microbiome of CRC patients differed from that of healthy controls. At the phylum level, the ratio of Firmicutes to Bacteroidetes was lower in the CRC patients. Microbial supernatants from *Blautia producta*, *Bifidobacterium adolescentis*, and *Bifidobacterium longum*, which were depleted in the fecal microbiome of CRC patients, inhibited the growth of CRC organoids. The inhibitory effect was not shown in the organoids from normal colon crypts. Butyric acid was found only in the microbial supernatants of *Bifidobacterium adolescentis* and *Bifidobacterium longum.* Isovaleric acid and acetic acid were more abundant in the supernatants of *Parabacteroides distasonis* and *Bacteroides ovatus*, which were more abundant in the fecal microbiome of CRC patients. In transcriptome analysis, CYP1A1 was the most upregulated gene by treatment with CRC-depleted microbial supernatants, and DKK4 was expressed at a higher level than other genes in CRC-abundant bacterial supernatants. The CRC-abundant bacteria group upregulated TGF-β and ROS pathways in normal colon organoids. The CRC-depleted bacteria group downregulated ROS pathways and upregulated PIK3_AKT_mTOR signaling pathways.

In conclusion, metabolomes secreted by the gut microbiome, especially butyrate-producing bacteria, may inhibit CRC tumor growth. Further studies are warranted to confirm that enhancing the beneficial metabolome level in the colon may prevent or disturb CRC progression.

Bibliography

Arrieta, M. C., Stiemsma, L. T., Amenyogbe, N., Brown, E. M., & Finlay, B. (2014). The intestinal microbiome in early life: health and disease. *Front Immunol, 5*, 427. doi:10.3389/fimmu.2014.00427

Bokulich, N. A., Kaehler, B. D., Rideout, J. R., Dillon, M., Bolyen, E., Knight, R., . . . Gregory Caporaso, J. (2018). Optimizing taxonomic classification of marker-gene amplicon sequences with QIIME 2's q2-feature-classifier plugin. *Microbiome, 6*(1), 90. doi:10.1186/s40168-018-0470-z

Bolger, A. M., Lohse, M., & Usadel, B. (2014). Trimmomatic: a flexible trimmer for Illumina sequence data. *Bioinformatics, 30*(15), 2114-2120. doi:10.1093/bioinformatics/btu170

Bolyen, E., Rideout, J. R., Dillon, M. R., Bokulich, N. A., Abnet, C. C., Al-Ghalith, G. A., . . . Caporaso, J. G. (2019). Reproducible, interactive, scalable and extensible microbiome data science using QIIME 2. *Nat Biotechnol, 37*(8), 852-857. doi:10.1038/s41587-019-0209-9

Bosch, S., Berkhout, D. J., Ben Larbi, I., de Meij, T. G., & de Boer, N. K. (2019). Fecal volatile organic compounds for early detection of colorectal cancer: where are we now? *J Cancer Res Clin Oncol, 145*(1), 223-234. doi:10.1007/s00432-018-2821-3

Brown, A. J., Goldsworthy, S. M., Barnes, A. A., Eilert, M. M., Tcheang, L., Daniels, D., . . . Dowell, S. J. (2003). The Orphan G protein-coupled receptors GPR41 and GPR43 are activated by propionate and other short chain carboxylic acids. *J Biol Chem, 278*(13), 11312-11319. doi:10.1074/jbc.M211609200

Callahan, B. J., McMurdie, P. J., Rosen, M. J., Han, A. W., Johnson, A. J., & Holmes, S. P. (2016). DADA2: High-resolution sample inference from Illumina amplicon data. *Nat Methods, 13*(7), 581-583. doi:10.1038/nmeth.3869

Chang, J. H., Shim, Y. Y., Cha, S. K., Reaney, M. J. T., & Chee, K. M. (2012). Effect of Lactobacillus acidophilus KFRI342 on the development of chemically induced precancerous growths in the rat colon. *J Med Microbiol, 61*(Pt 3), 361-368. doi:10.1099/jmm.0.035154-0

Chung, L., Thiele Orberg, E., Geis, A. L., Chan, J. L., Fu, K., DeStefano Shields, C. E., . . . Housseau, F. (2018). Bacteroides fragilis Toxin Coordinates a Pro-carcinogenic Inflammatory Cascade via Targeting of Colonic Epithelial Cells. *Cell Host Microbe, 23*(2), 203-214 e205. doi:10.1016/j.chom.2018.01.007

Dekker, E., Tanis, P. J., Vleugels, J. L. A., Kasi, P. M., & Wallace, M. B. (2019). Colorectal cancer. *Lancet, 394*(10207), 1467-1480. doi:10.1016/S0140-6736(19)32319-0

Fellows, R., Denizot, J., Stellato, C., Cuomo, A., Jain, P., Stoyanova, E., . . . Varga-Weisz, P. (2018). Microbiota derived short chain fatty acids promote histone crotonylation in the colon through histone

deacetylases. *Nat Commun, 9*(1), 105. doi:10.1038/s41467-017-02651-5

Feng, Q., Liang, S., Jia, H., Stadlmayr, A., Tang, L., Lan, Z., . . . Wang, J. (2015). Gut microbiome development along the colorectal adenoma-carcinoma sequence. *Nat Commun, 6*, 6528. doi:10.1038/ncomms7528

Flemer, B., Lynch, D. B., Brown, J. M., Jeffery, I. B., Ryan, F. J., Claesson, M. J., . . . O'Toole, P. W. (2017). Tumour-associated and non-tumour-associated microbiota in colorectal cancer. *Gut, 66*(4), 633-643. doi:10.1136/gutjnl-2015-309595

Kang, M. J., Jung, K. W., Bang, S. H., Choi, S. H., Park, E. H., Yun, E. H., . . . Community of Population-Based Regional Cancer, R. (2023). Cancer Statistics in Korea: Incidence, Mortality, Survival, and Prevalence in 2020. *Cancer Res Treat, 55*(2), 385-399. doi:10.4143/crt.2023.447

Khazaie, K., Zadeh, M., Khan, M. W., Bere, P., Gounari, F., Dennis, K., . . . Mohamadzadeh, M. (2012). Abating colon cancer polyposis by Lactobacillus acidophilus deficient in lipoteichoic acid. *Proc Natl Acad Sci U S A, 109*(26), 10462-10467. doi:10.1073/pnas.1207230109

Kim, D., Langmead, B., & Salzberg, S. L. (2015). HISAT: a fast spliced aligner with low memory requirements. *Nat Methods, 12*(4), 357-360. doi:10.1038/nmeth.3317

Kim, Y., Lee, D., Kim, D., Cho, J., Yang, J., Chung, M., . . . Ha, N. (2008). Inhibition of proliferation in colon cancer cell lines and harmful enzyme activity of colon bacteria by Bifidobacterium adolescentis SPM0212. *Arch Pharm Res, 31*(4), 468-473. doi:10.1007/s12272-001-1180-y

Kostic, A. D., Chun, E., Robertson, L., Glickman, J. N., Gallini, C. A., Michaud, M., . . . Garrett, W. S. (2013). Fusobacterium nucleatum potentiates intestinal tumorigenesis and modulates the tumor-immune microenvironment. *Cell Host Microbe, 14*(2), 207-215. doi:10.1016/j.chom.2013.07.007

Liu, Z., Qin, H., Yang, Z., Xia, Y., Liu, W., Yang, J., . . . Zheng, Q. (2011). Randomised clinical trial: the effects of perioperative probiotic treatment on barrier function and post-operative infectious complications in colorectal cancer surgery - a double-blind study. *Aliment Pharmacol Ther, 33*(1), 50-63. doi:10.1111/j.1365-2036.2010.04492.x

Long, X., Wong, C. C., Tong, L., Chu, E. S. H., Ho Szeto, C., Go, M. Y. Y., . . . Yu, J. (2019). Peptostreptococcus anaerobius promotes colorectal carcinogenesis and modulates tumour immunity. *Nat Microbiol, 4*(12), 2319-2330. doi:10.1038/s41564-019-0541-3

Louis, P., & Flint, H. J. (2017). Formation of propionate and butyrate by the human colonic microbiota. *Environ Microbiol, 19*(1), 29-41. doi:10.1111/1462-2920.13589

Louis, P., Hold, G. L., & Flint, H. J. (2014). The gut microbiota, bacterial metabolites and colorectal cancer. *Nat Rev Microbiol, 12*(10), 661-672. doi:10.1038/nrmicro3344

Martinez, F. D. (2014). The human microbiome. Early life determinant of

health outcomes. *Ann Am Thorac Soc, 11 Suppl 1*(Suppl 1), S7-12. doi:10.1513/AnnalsATS.201306-186MG

Maslowski, K. M., Vieira, A. T., Ng, A., Kranich, J., Sierro, F., Yu, D., . . . Mackay, C. R. (2009). Regulation of inflammatory responses by gut microbiota and chemoattractant receptor GPR43. *Nature, 461*(7268), 1282-1286. doi:10.1038/nature08530

Mehta, R. S., Nishihara, R., Cao, Y., Song, M., Mima, K., Qian, Z. R., . . . Ogino, S. (2017). Association of Dietary Patterns With Risk of Colorectal Cancer Subtypes Classified by Fusobacterium nucleatum in Tumor Tissue. *JAMA Oncol, 3*(7), 921-927. doi:10.1001/jamaoncol.2016.6374

Mohamadzadeh, M., Pfeiler, E. A., Brown, J. B., Zadeh, M., Gramarossa, M., Managlia, E., . . . Klaenhammer, T. R. (2011). Regulation of induced colonic inflammation by Lactobacillus acidophilus deficient in lipoteichoic acid. *Proc Natl Acad Sci U S A, 108 Suppl 1*(Suppl 1), 4623-4630. doi:10.1073/pnas.1005066107

Nakatsu, G., Li, X., Zhou, H., Sheng, J., Wong, S. H., Wu, W. K., . . . Sung, J. J. (2015). Gut mucosal microbiome across stages of colorectal carcinogenesis. *Nat Commun, 6*, 8727. doi:10.1038/ncomms9727

Olszak, T., An, D., Zeissig, S., Vera, M. P., Richter, J., Franke, A., . . . Blumberg, R. S. (2012). Microbial exposure during early life has persistent effects on natural killer T cell function. *Science, 336*(6080), 489-493. doi:10.1126/science.1219328

Parada Venegas, D., De la Fuente, M. K., Landskron, G., Gonzalez, M. J., Quera, R., Dijkstra, G., . . . Hermoso, M. A. (2019). Short Chain Fatty Acids (SCFAs)-Mediated Gut Epithelial and Immune Regulation and Its Relevance for Inflammatory Bowel Diseases. *Front Immunol, 10*, 277. doi:10.3389/fimmu.2019.00277

Pertea, M., Pertea, G. M., Antonescu, C. M., Chang, T. C., Mendell, J. T., & Salzberg, S. L. (2015). StringTie enables improved reconstruction of a transcriptome from RNA-seq reads. *Nat Biotechnol, 33*(3), 290-295. doi:10.1038/nbt.3122

Quast, C., Pruesse, E., Yilmaz, P., Gerken, J., Schweer, T., Yarza, P., . . . Glockner, F. O. (2013). The SILVA ribosomal RNA gene database project: improved data processing and web-based tools. *Nucleic Acids Res, 41*(Database issue), D590-596. doi:10.1093/nar/gks1219

Rubinstein, M. R., Wang, X., Liu, W., Hao, Y., Cai, G., & Han, Y. W. (2013). Fusobacterium nucleatum promotes colorectal carcinogenesis by modulating E-cadherin/beta-catenin signaling via its FadA adhesin. *Cell Host Microbe, 14*(2), 195-206. doi:10.1016/j.chom.2013.07.012

Siegel, R. L., Miller, K. D., Wagle, N. S., & Jemal, A. (2023). Cancer statistics, 2023. *CA Cancer J Clin, 73*(1), 17-48. doi:10.3322/caac.21763

Singh, N., Gurav, A., Sivaprakasam, S., Brady, E., Padia, R., Shi, H., . . . Ganapathy, V. (2014). Activation of Gpr109a, receptor for niacin and the commensal metabolite butyrate, suppresses colonic inflammation and carcinogenesis. *Immunity, 40*(1), 128-139. doi:10.1016/j.immuni.2013.12.007

Sinicrope, F. A. (2022). Increasing Incidence of Early-Onset Colorectal Cancer. *N Engl J Med, 386*(16), 1547-1558. doi:10.1056/NEJMra2200869

Sommer, F., & Backhed, F. (2013). The gut microbiota--masters of host development and physiology. *Nat Rev Microbiol, 11*(4), 227-238. doi:10.1038/nrmicro2974

Song, M. H., Park, J. W., Kim, M. J., Shin, Y. K., Kim, S. C., Jeong, S. Y., & Ku, J. L. (2022). Colon cancer organoids using monoclonal organoids established in four different lesions of one cancer patient reveal tumor heterogeneity and different real-time responsiveness to anti-cancer drugs. *Biomed Pharmacother, 152*, 113260. doi:10.1016/j.biopha.2022.113260

Thangaraju, M., Cresci, G. A., Liu, K., Ananth, S., Gnanaprakasam, J. P., Browning, D. D., . . . Ganapathy, V. (2009). GPR109A is a G-protein-coupled receptor for the bacterial fermentation product butyrate and functions as a tumor suppressor in colon. *Cancer Res, 69*(7), 2826-2832. doi:10.1158/0008-5472.CAN-08-4466

Vital, M., Howe, A. C., & Tiedje, J. M. (2014). Revealing the bacterial butyrate synthesis pathways by analyzing (meta)genomic data. *mBio, 5*(2), e00889. doi:10.1128/mBio.00889-14

Vogtmann, E., Hua, X., Zeller, G., Sunagawa, S., Voigt, A. Y., Hercog, R., . . . Sinha, R. (2016). Colorectal Cancer and the Human Gut Microbiome: Reproducibility with Whole-Genome Shotgun Sequencing. *PLoS One, 11*(5), e0155362. doi:10.1371/journal.pone.0155362

Wirbel, J., Pyl, P. T., Kartal, E., Zych, K., Kashani, A., Milanese, A., . . . Zeller, G. (2019). Meta-analysis of fecal metagenomes reveals global microbial signatures that are specific for colorectal cancer. *Nat Med, 25*(4), 679-689. doi:10.1038/s41591-019-0406-6

Yang, I., Corwin, E. J., Brennan, P. A., Jordan, S., Murphy, J. R., & Dunlop, A. (2016). The Infant Microbiome: Implications for Infant Health and Neurocognitive Development. *Nurs Res, 65*(1), 76-88. doi:10.1097/NNR.0000000000000133

Yang, Y., Weng, W., Peng, J., Hong, L., Yang, L., Toiyama, Y., . . . Ma, Y. (2017). Fusobacterium nucleatum Increases Proliferation of Colorectal Cancer Cells and Tumor Development in Mice by Activating Toll-Like Receptor 4 Signaling to Nuclear Factor-kappaB, and Up-regulating Expression of MicroRNA-21. *Gastroenterology, 152*(4), 851-866 e824. doi:10.1053/j.gastro.2016.11.018

Yatsunenko, T., Rey, F. E., Manary, M. J., Trehan, I., Dominguez-Bello, M. G., Contreras, M., . . . Gordon, J. I. (2012). Human gut microbiome viewed across age and geography. *Nature, 486*(7402), 222-227. doi:10.1038/nature11053

Zeller, G., Tap, J., Voigt, A. Y., Sunagawa, S., Kultima, J. R., Costea, P. I., . . . Bork, P. (2014). Potential of fecal microbiota for early-stage detection of colorectal cancer. *Mol Syst Biol, 10*(11), 766. doi:10.15252/msb.20145645

Zhang, M., Fan, X., Fang, B., Zhu, C., Zhu, J., & Ren, F. (2015). Effects of

Lactobacillus salivarius Ren on cancer prevention and intestinal microbiota in 1, 2-dimethylhydrazine-induced rat model. *J Microbiol, 53*(6), 398-405. doi:10.1007/s12275-015-5046-z

Zhu, J., Zhu, C., Ge, S., Zhang, M., Jiang, L., Cui, J., & Ren, F. (2014). Lactobacillus salivarius Ren prevent the early colorectal carcinogenesis in 1, 2-dimethylhydrazine-induced rat model. *J Appl Microbiol, 117*(1), 208-216. doi:10.1111/jam.12499

Figures and Tables

Figure 1. Schematic diagram of the study. The overall flow chart was miniaturized.

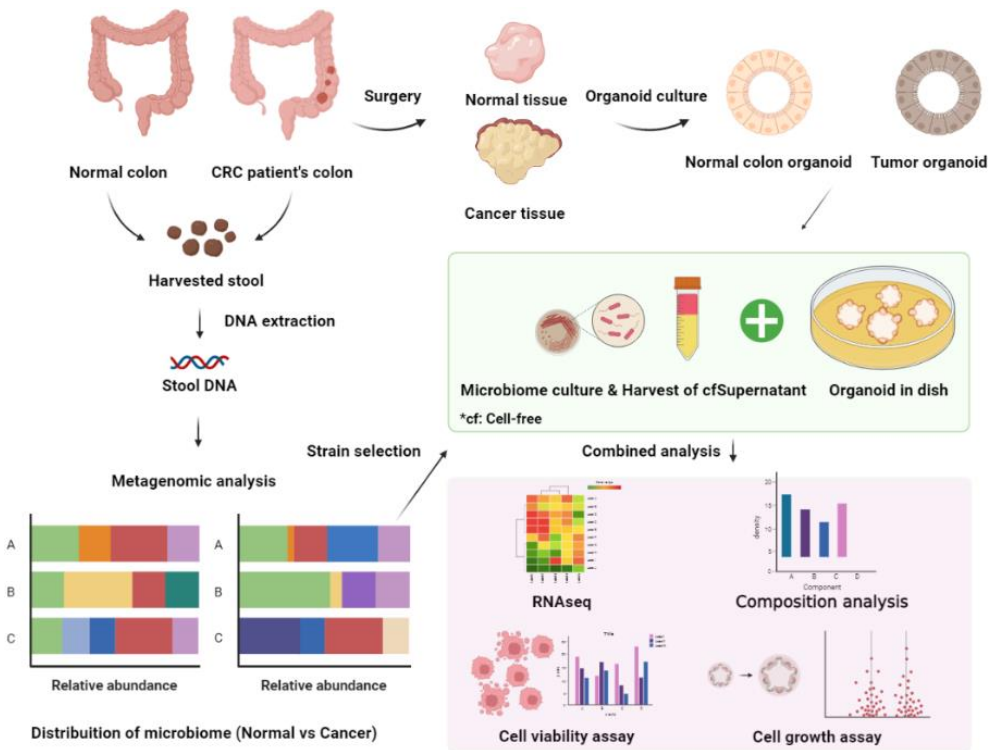

Figure 2A. TNM classification and the AJCC stage of CRC (n=40)

Cancer stage	Type	n (%)
T classification	T1	2 (5%)
	T2	2 (5%)
	T3	28 (70%)
	T4	8 (20%)
N classification	N0	19 (47.5%)
	N1	11 (27.5%)
	N2	10 (25%)
M classification	M0	29 (72.5%)
	M1	11(27.5%)
AJCC Stage	I	3 (7.5%)
	II	14 (35%)
	III	12 (30%)
	IV	11 (27.5%)

Abbreviations: TNM=tumor, node, and metastasis; AJCC=the American Joint Committee on Cancer

Figure 2B. Alpha (intra-sample) diversity from healthy controls and CRC patients was analyzed by Chao1, Shannon, and Simpson methods

Chao1 p-value=0.513

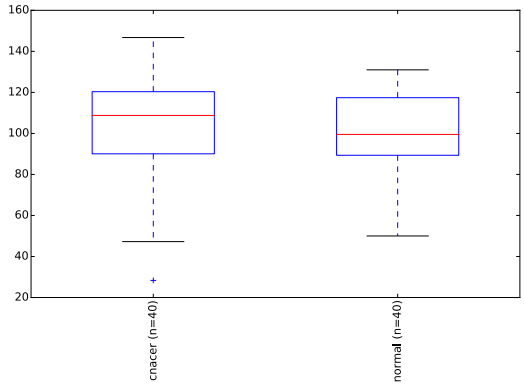

Shannon. p-value=0.04

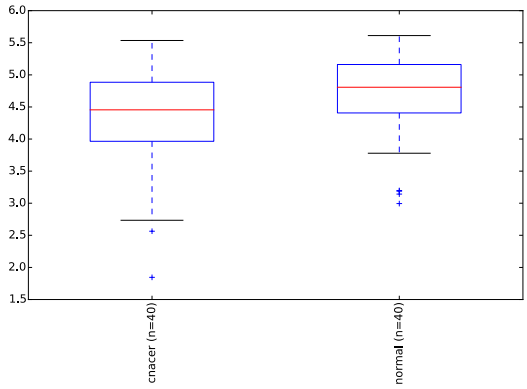

Simpson. p-value=0.109

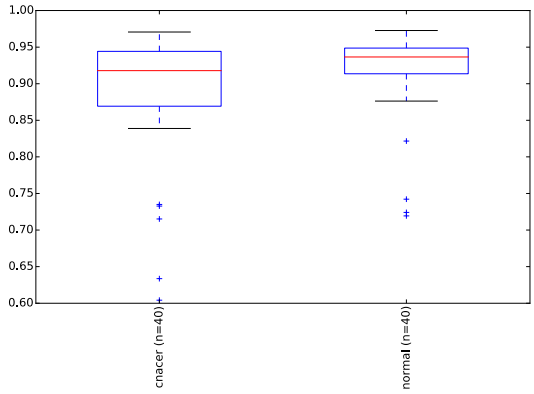

Figure 2C. Microbial taxonomic distribution data from healthy controls and CRC patients were patterned by Bray−Curtis, weighted UniFrac, and unweighted UniFrac analysis

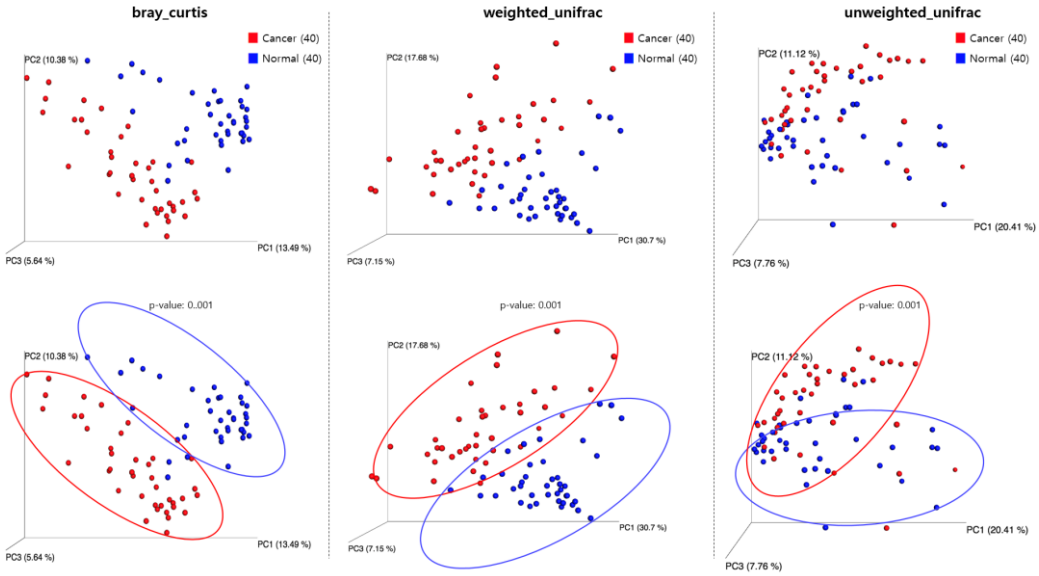

Figure 2D. The microbial distribution of individual samples at the phylum level

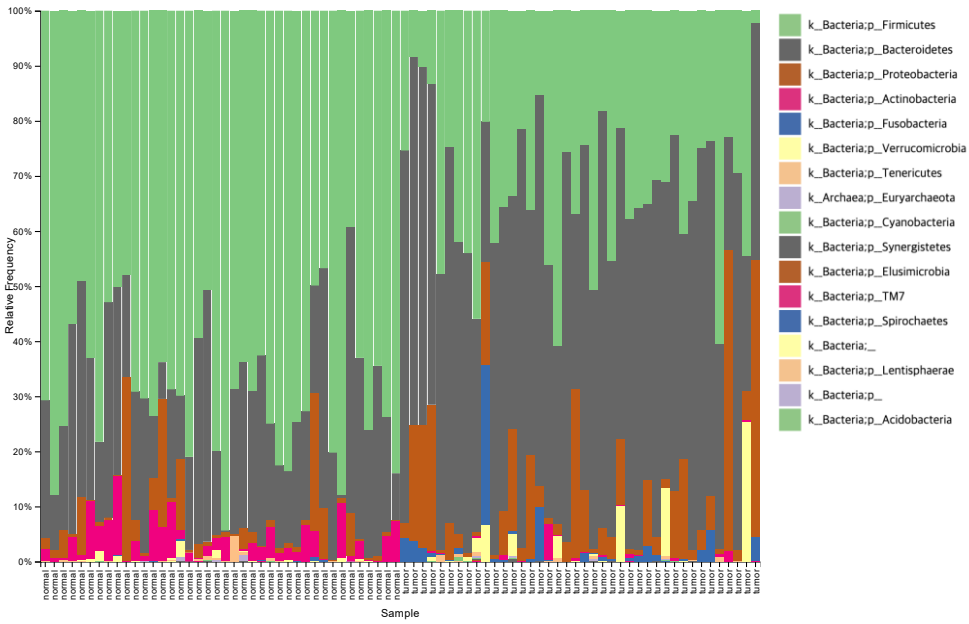

Figure 2E. The linear discriminant analysis (LDA) effect size (LEfSe) analysis. The LDA score was calculated to present the portions of difference between samples of cancer-specific strains in comparison with healthy controls

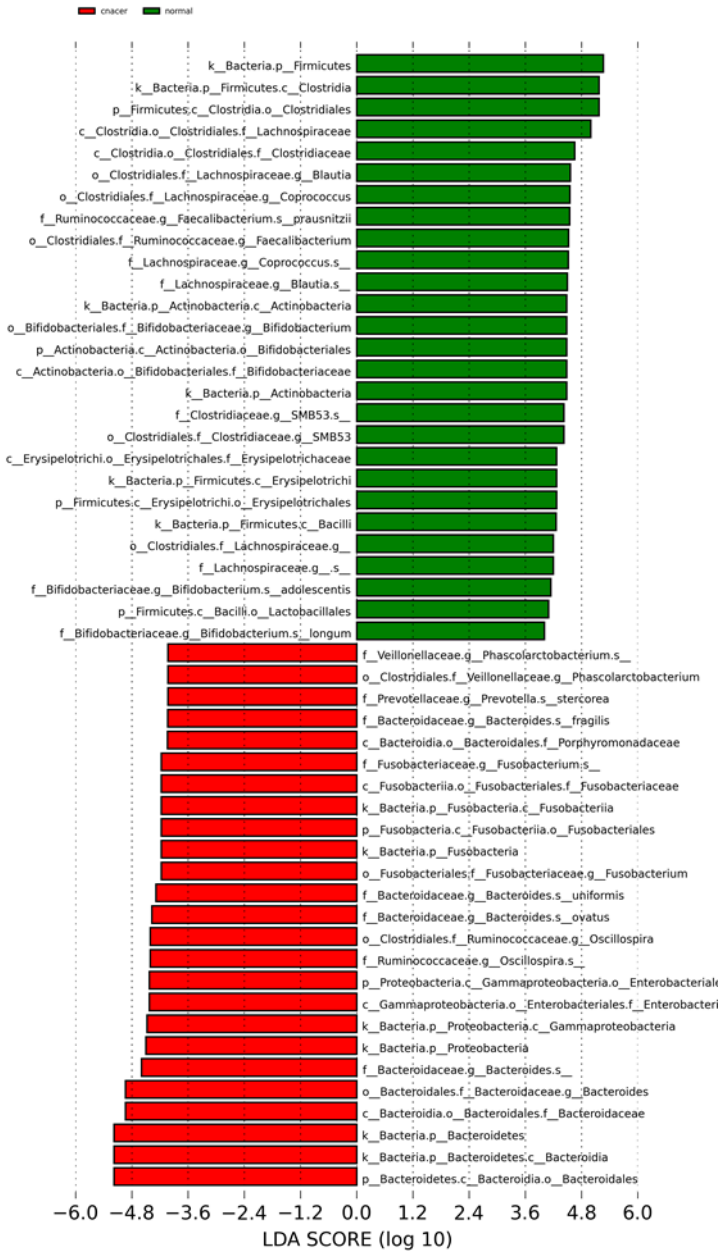

Figure 2F. Cladogram

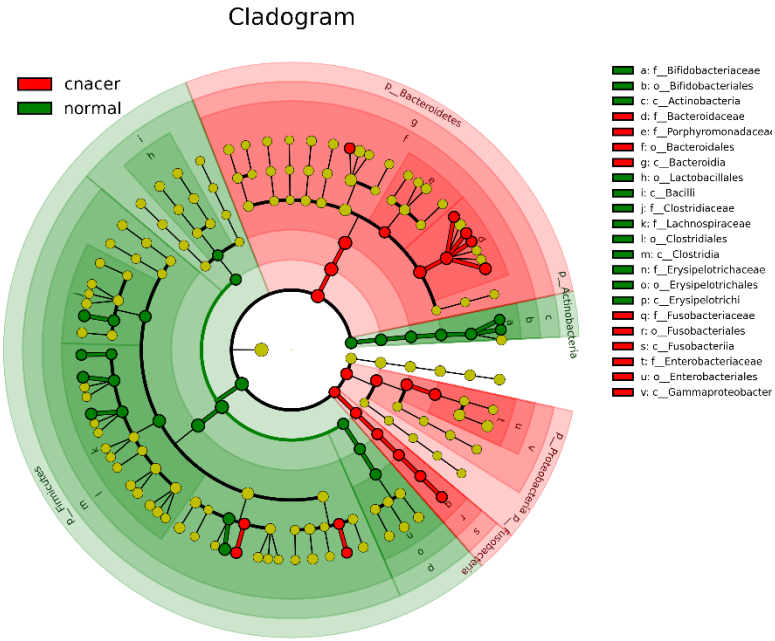

Table 1. Species that are more abundant in healthy controls vs. CRC patients

More abundant in healthy control		More abundant in CRC patients	
Genus	Species	Genus	Species
g__Blautia	*s__obeum*	*g__Bacteroides*	*s__ovatus*
g__Blautia	*s__producta*	*g__Parabacteroides*	*s__distasonis*
g__Dorea	*s__longicatena*	*g__Bacteroides*	*s__uniformis*
g__Faecalibacterium	*s__prausnitzii*	*g__Parabacteroides*	*s__gordonii*
g__Clostridium	*s__celatum*	*g__Morganella*	*s__morganii*
g__Bifidobacterium	*s__longum*	*g__Clostridium*	*s__symbiosum*
g__Bifidobacterium	*s__adolescentis*	*g__Bacteroides*	*s__fragilis*
g__Gemmiger	*s__formicilis*	*g__Porphyromonas*	*s__endodontalis*
g__Lactobacillus	*s__ruminis*	*g__Prevotella*	*s__intermedia*
g__Luminococcus	*s__callidus*	*g__Peptostreptococcus*	*s__anaerobius*
g__Roseburia	*s__faecis*	*g__Clostridium*	*s__hathewayi*
g__Ruminococcus	*s__bromii*	*g__Veillonella*	*s__parvula*
g__Coprococcus	*s__eutactus*	*g__Campylobacter*	*s__rectus*

Figure 3A. Bright field image of established CRC organoid lines

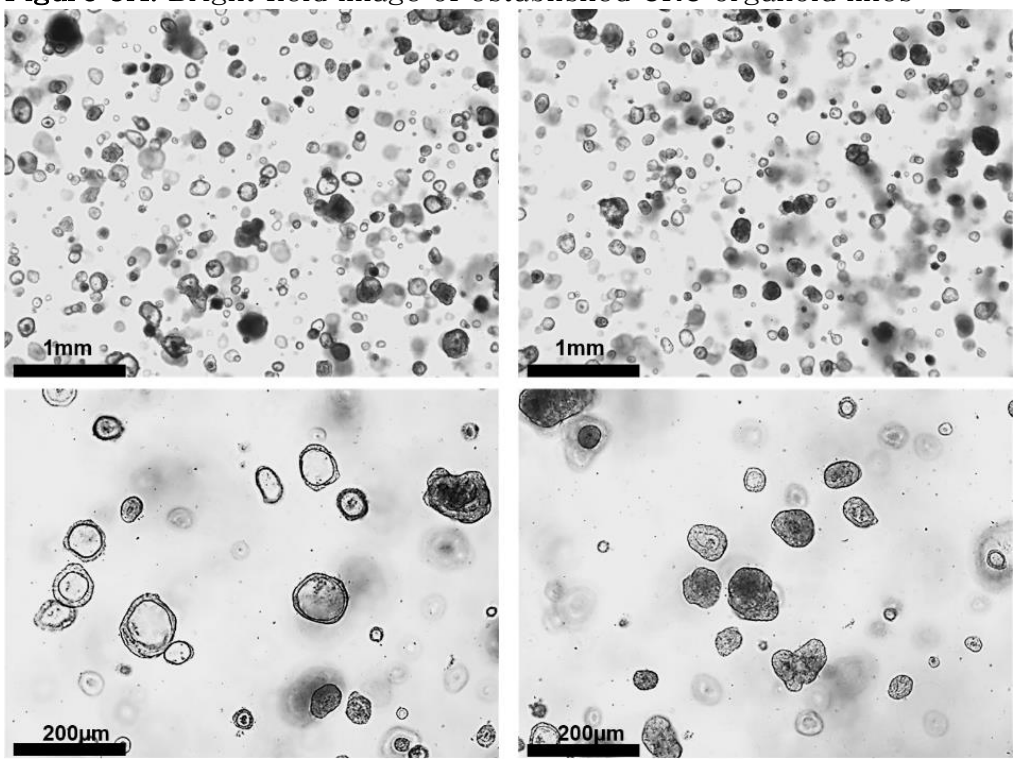

Figure 3B. Bright field image of established normal colon epithelium organoid lines

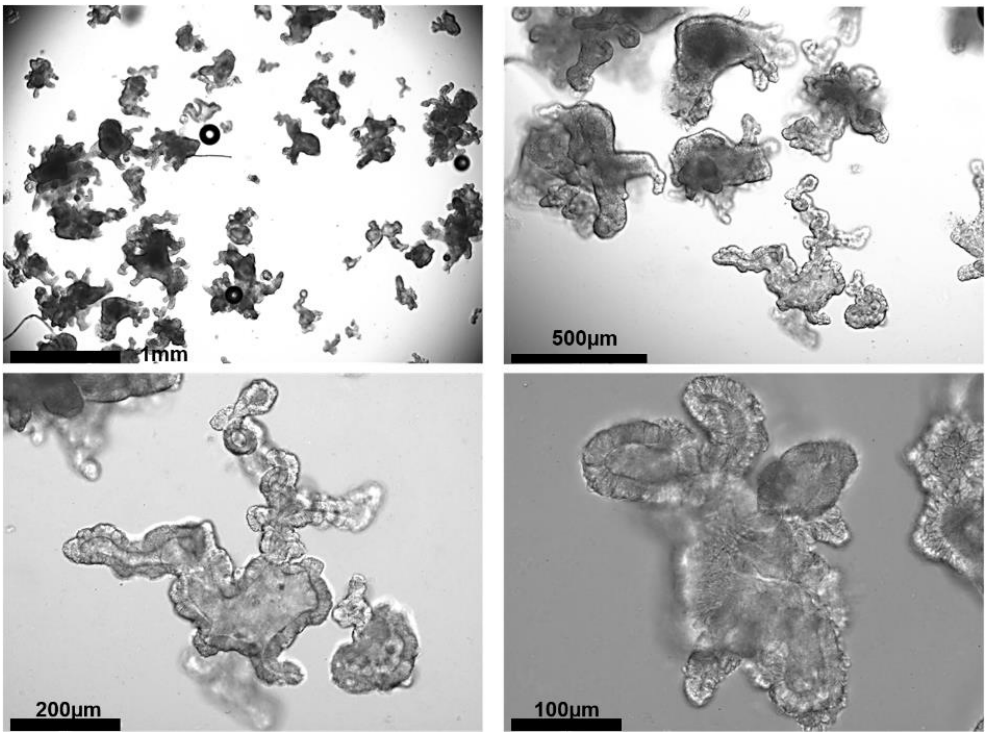

Figure 4A. SNU-7237-TO was treated with each microbial supernatant, organoid plain medium, and bacteria plain medium. The culture state of organoids after 3-, 6-, and 12-days was captured with optical microscopy

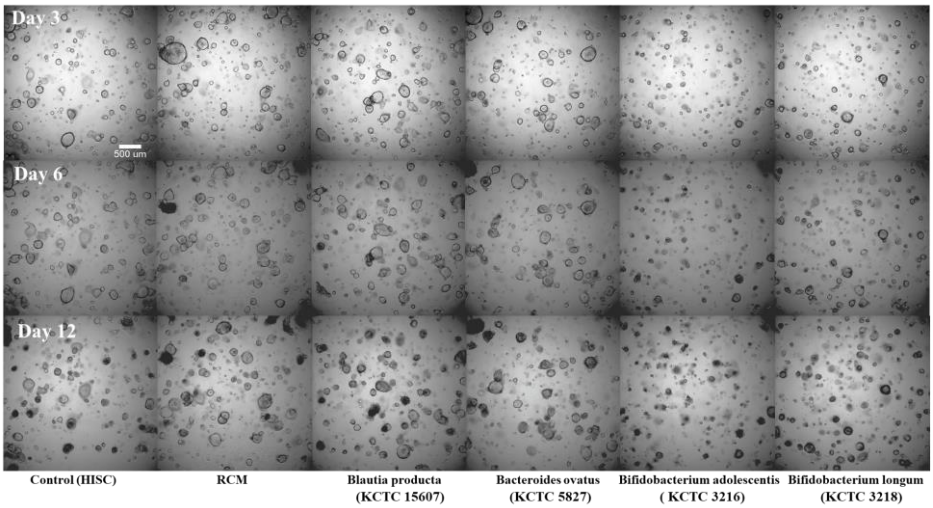

Figure 4B. SNU-7390S3-TO was treated with each microbial supernatant, organoid plain medium, and bacteria plain medium. The culture state of organoids after 3-, 6-, and 12-days was captured with optical microscopy

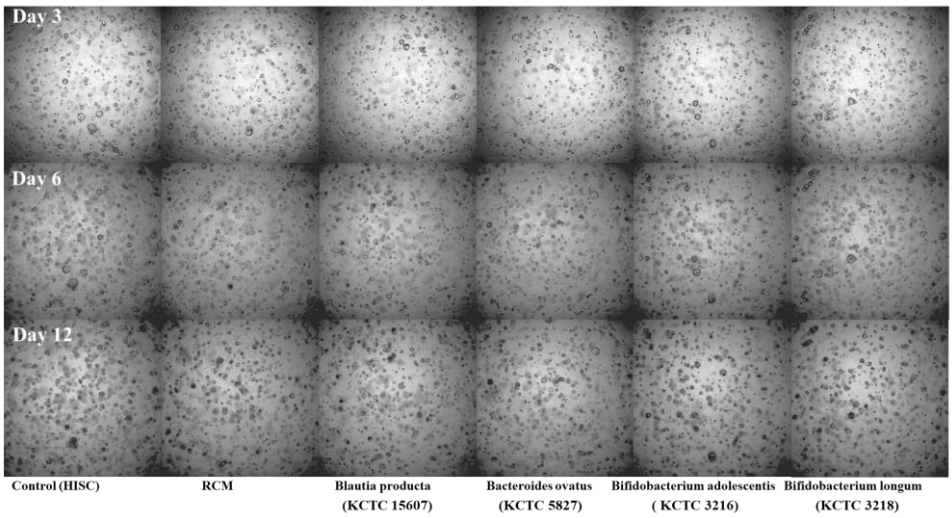

Figure 4C. Viable tumor organoid cells after treatment with culture metabolites visualized as a bar plot based on the relative light unit (RLU) parameter

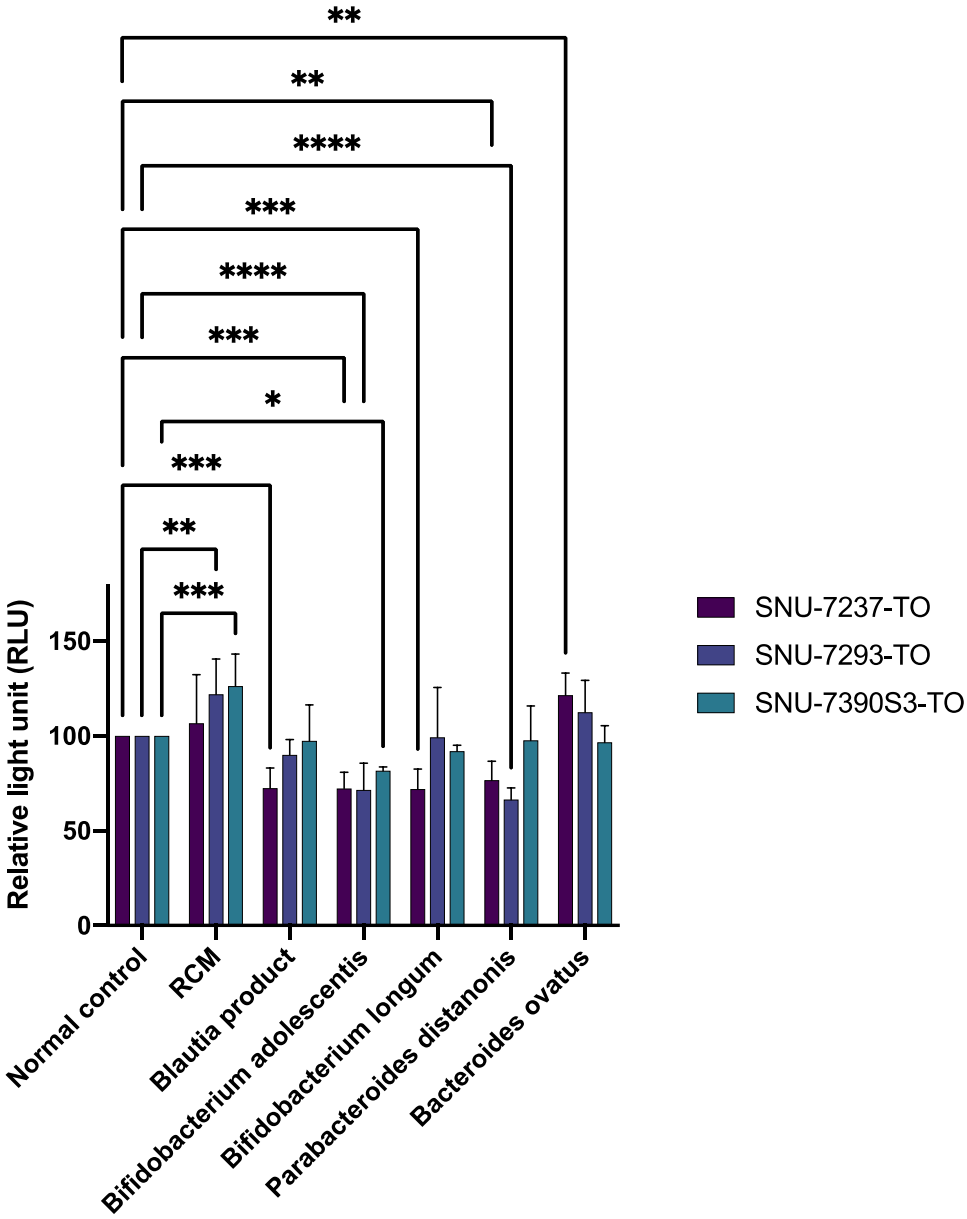

Figure 4D. Viable normal colon epithelium organoid cells after treatment with culture metabolites visualized as a bar plot based on the relative light unit (RLU) parameter.

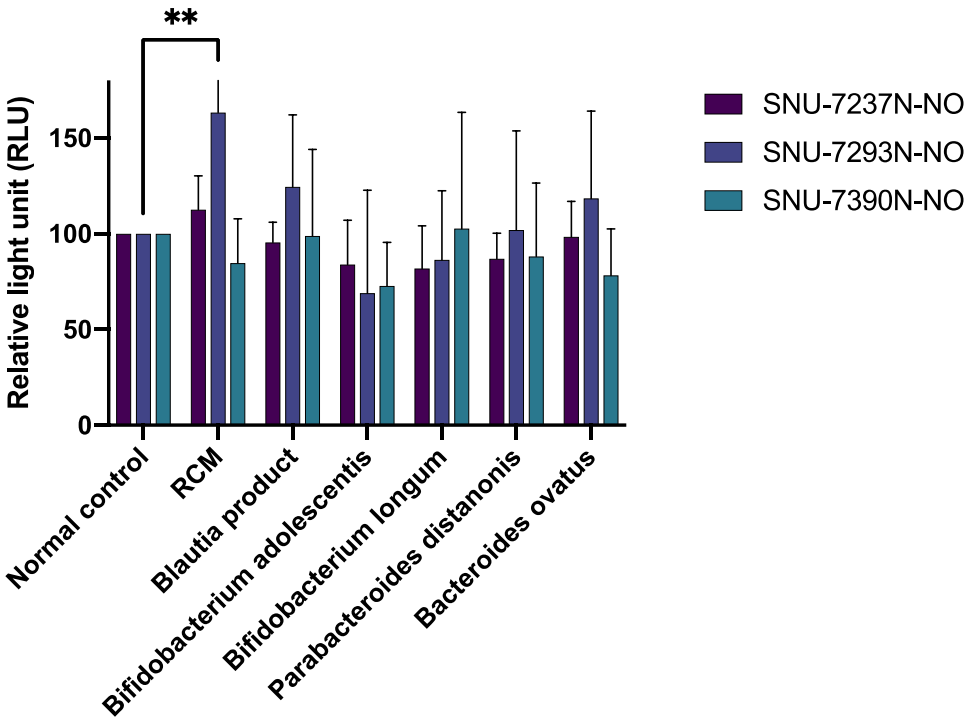

Figure 4E. Perimeters in the captured images of SNU-7237-TO which is treated by each bacterial supernatant, bacterial culture medium and organoid medium (control).

- *Bifidobacterium adolescentis* vs. HISC (control)

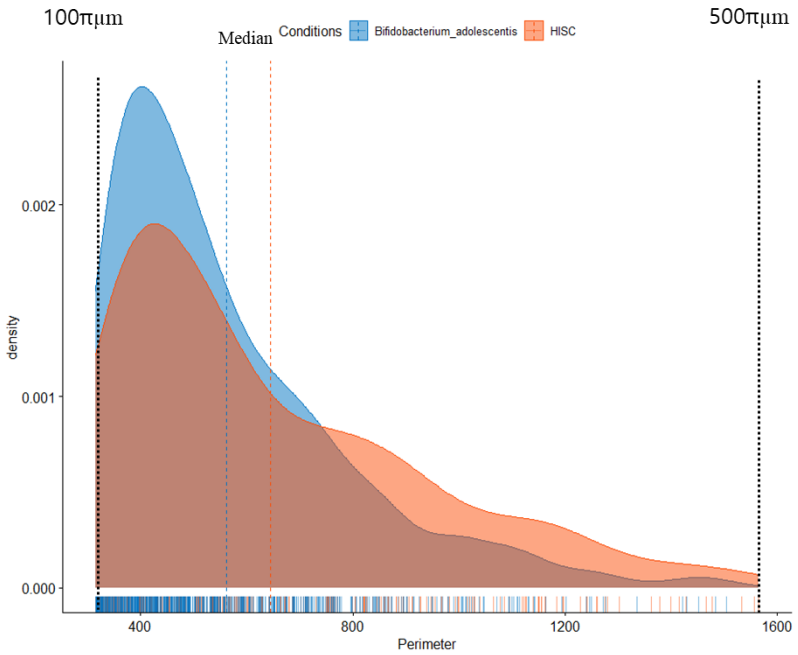

- *Bifidobacterium longum* vs. HISC (control)

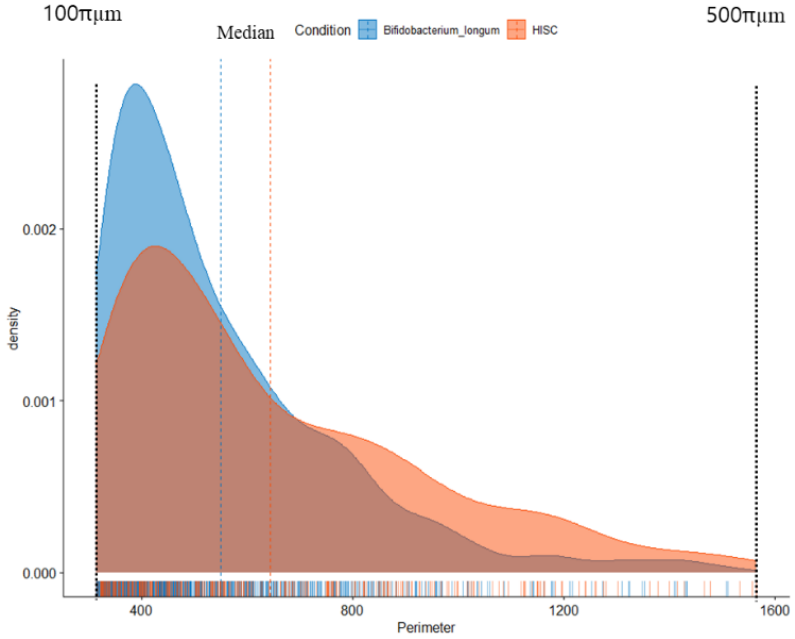

- RCM (Reinforced Clostridial Medium) vs. HISC (control)

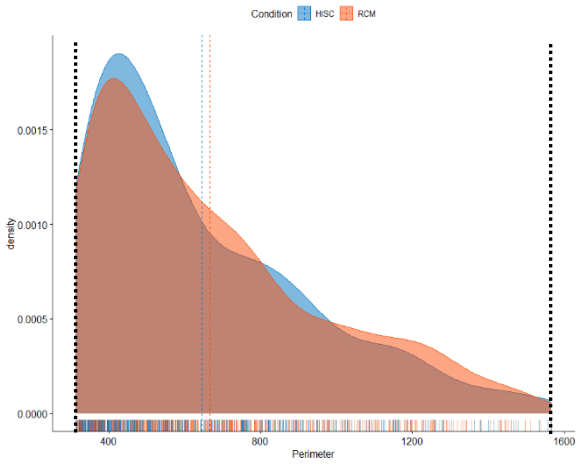

- *Blautia producta* vs. HISC (control)

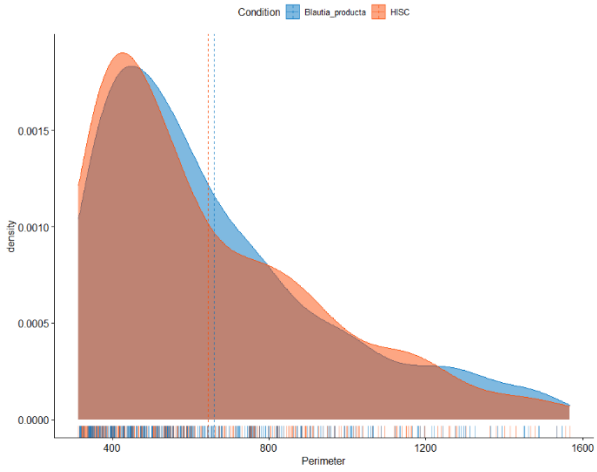

- *Bacteroides ovatus* vs. HISC (control)

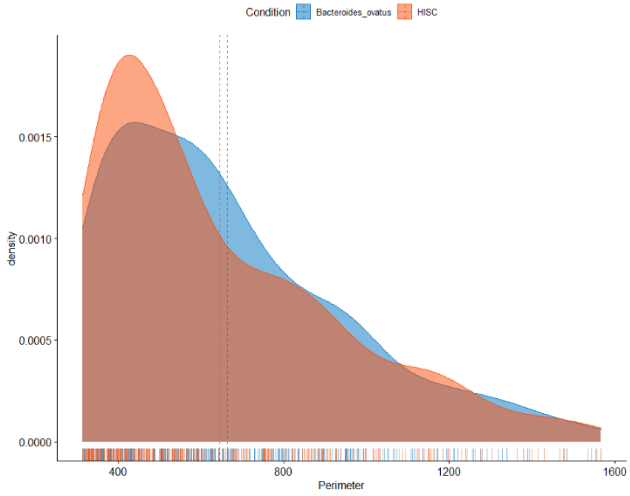

Figure 5A. RNA sequencing analysis. The Bifidobacterium group separated from the CRC-abundant group (*Parabacteroides distasonis* and Bacteroides ovatus) is shown on the PCA plot.

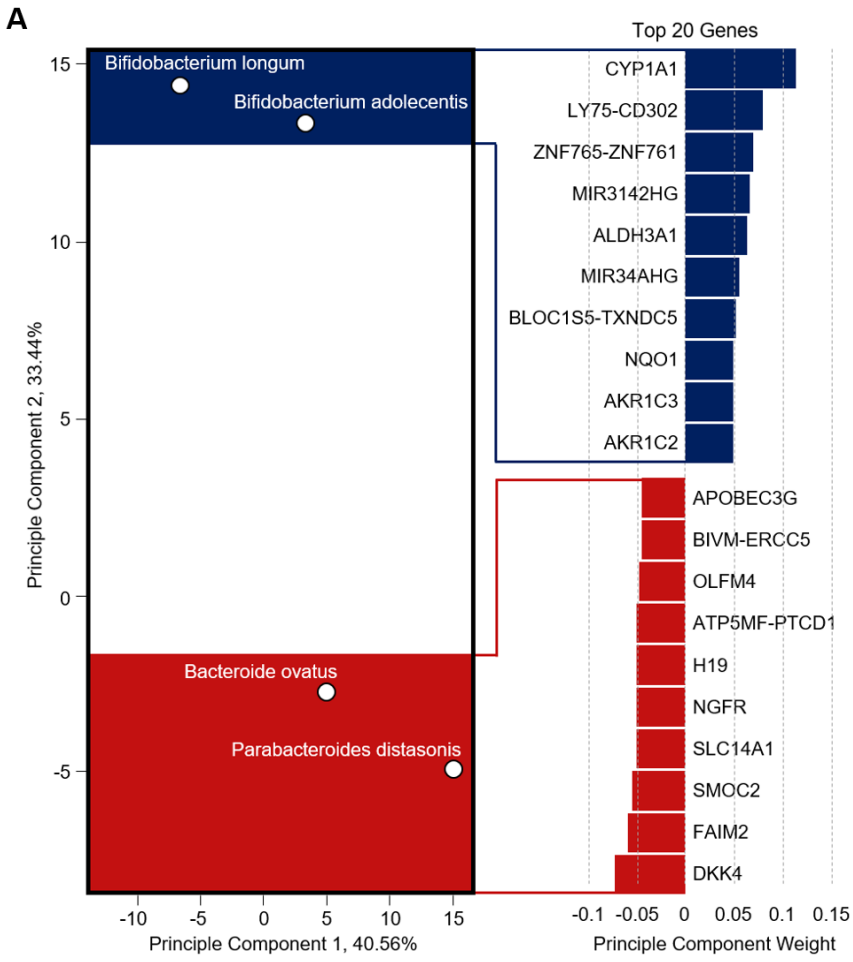

Figure 5B. RNA sequencing analysis

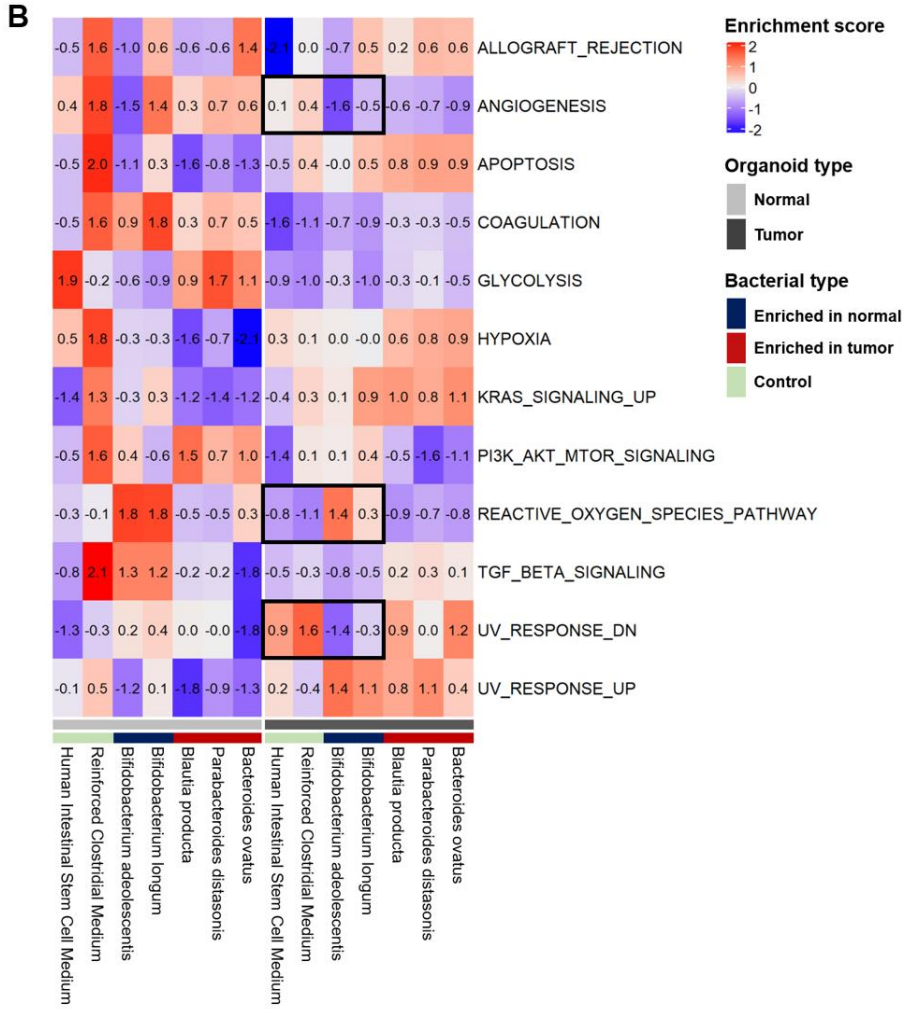

Figure 6A. Component analysis. *B. adolescentis* and *B. Longum* were considered as healthy controls while data of *P. distasonis* and *B. ovatus* were assumed as cancer patients. Relative portions of each subtype in amino acids, carbohydrates, fatty acids, lipids, organic acids, purines, and pyrimidines, etc. were calculated through data normalization.

❖ Heat-map analysis (VIP>1.0)

0 1 2

	3216	3218	5751	5827	Normal subject	Cancer subject	
Amino acids	1.08	1.08	0.85	0.99	1.08	0.92	Alanine a
	1.14	1.28	0.75	0.83	1.21	0.79	Valine a
	1.10	1.35	0.74	0.82	1.22	0.78	Isoleucine a
	1.12	1.30	0.75	0.83	1.21	0.79	Proline
	1.15	1.21	0.74	0.90	1.18	0.82	Glycine a
	1.14	1.31	0.73	0.82	1.23	0.77	Serine
	1.12	1.33	0.69	0.86	1.22	0.78	Threonine
	1.29	1.65	0.38	0.67	1.47	0.53	Homoserine
	1.65	1.47	0.77	0.10	1.56	0.44	Aspartic acid a
	1.10	1.02	0.94	0.94	1.06	0.94	Pyroglutamic acid
	0.26	0.26	1.07	2.41	0.26	1.74	Gamma-Aminobutyric acid (GABA) a
	1.51	1.56	0.77	0.15	1.54	0.46	Glutamic acid a
	1.23	1.26	0.71	0.80	1.25	0.75	Phenylalanine a
	1.65	1.97	0.36	0.03	1.81	0.19	Asparagine a
	1.18	1.47	0.78	0.57	1.32	0.68	Glutamine a
	1.25	1.74	0.41	0.60	1.50	0.50	Ornithine
	1.30	1.17	0.66	0.87	1.23	0.77	Lysine
	1.77	1.60	0.50	0.13	1.68	0.32	Tyrosine a
	1.06	1.68	0.58	0.69	1.37	0.63	Tryptophan a
	0.12	0.39	2.11	1.37	0.26	1.74	Cystine
Carbohydrates	0.85	0.82	1.15	1.17	0.84	1.16	Glycerol a
	2.10	1.00	0.39	0.50	1.55	0.45	Erythronic acid a
	1.23	0.50	1.27	1.00	0.86	1.14	Arabinitol
	2.15	1.23	0.26	0.36	1.69	0.31	Ribonic acid a
	1.31	0.10	1.34	1.25	0.71	1.29	Glucose
	1.42	1.74	0.37	0.48	1.58	0.42	Gluconic acid a
	2.03	1.65	0.13	0.19	1.84	0.16	Galactaric acid a
	0.86	0.83	1.13	1.17	0.85	1.15	myo-Inositol a
	3.75	0.07	0.10	0.08	1.91	0.09	Sucrose
	1.59	0.01	1.14	1.26	0.80	1.20	Maltose
Fatty acids & Lipids	0.44	0.17	1.87	1.53	0.30	1.70	Valeric acid or Isovaleric acid or 2-Methylbutyric acid a
	1.22	1.60	0.56	0.62	1.41	0.59	α-Hydroxyvaleric acid a
	0.73	0.84	1.26	1.17	0.79	1.21	4-Hydroxybutyric acid a
	1.10	2.30	0.20	0.39	1.70	0.30	2-Hydroxy-3-methylpentanoic acid a
	1.72	1.60	0.34	0.34	1.66	0.34	3-Hydroxymethylglutaric acid a
	1.31	1.33	0.73	0.62	1.32	0.68	Glycerophosphoric acid a
	1.24	0.01	1.37	1.38	0.63	1.37	MG(16:0/0:0/0:0) a
	1.22	0.01	1.40	1.37	0.61	1.39	MG(0:0/18:0/0:0) a

	3216	3218	5751	5827	Normal subject	Cancer subject	
Organic acids	0.36	0.55	1.18	1.90	0.46	1.54	Pyruvic acid a
	1.24	1.18	0.63	0.95	1.21	0.79	Glycolic acid a
	1.34	1.92	0.34	0.40	1.63	0.37	2-Hydroxybutyric acid a
	1.53	1.27	0.56	0.63	1.40	0.60	Oxalic acid a
	1.53	1.84	0.22	0.41	1.69	0.31	Malonic acid a
	0.55	0.61	1.37	1.48	0.58	1.42	Succinic acid a
	1.27	1.41	0.68	0.63	1.34	0.66	Dihydroxyisobutyric acid a
	0.60	0.65	1.36	1.39	0.62	1.38	Fumaric acid a
	1.83	1.44	0.38	0.36	1.63	0.37	Deoxytetronic acid a
	0.90	0.02	1.96	1.13	0.46	1.54	Malic acid a
	2.00	1.64	0.18	0.18	1.82	0.18	Citric acid a
Purines and pyrimidines	0.43	0.01	2.25	1.31	0.22	1.78	Inosine a
	2.97	0.17	0.63	0.23	1.57	0.43	Adenosine
	0.92	0.39	0.98	1.71	0.65	1.35	Uracil a
	1.94	0.53	0.74	0.79	1.24	0.76	Uridine
Etc.	0.90	0.79	1.04	1.28	0.84	1.16	1,3-Propanediol a
	1.63	1.40	0.45	0.53	1.51	0.49	2-Furoic acid a
	1.29	1.33	0.65	0.73	1.31	0.69	Benzoic acid a
	1.18	1.08	0.86	0.88	1.13	0.87	Phosphoric acid
	0.26	3.43	0.17	0.14	1.85	0.15	Pyruvic acid a

Figure 6B. The concentration of six short-chain fatty acids in each subjected sample

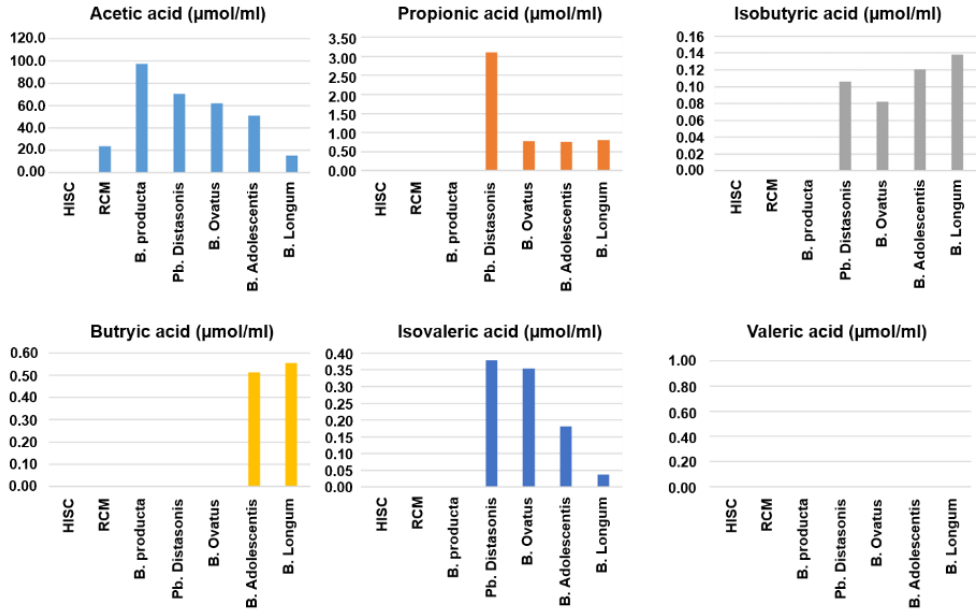

Figure 6C. Metabolomic distances between normal and cancer patients were performed for PCA (left) and OPLS-DA (right) PCA; R2X (cum): 0.657, Q2 (cum): 0.301, and OPLS-DA; R2X (cum): 0.608, R2Y (cum): 1, Q2 (cum): 0.938, and ANOVA p-value < 0.05

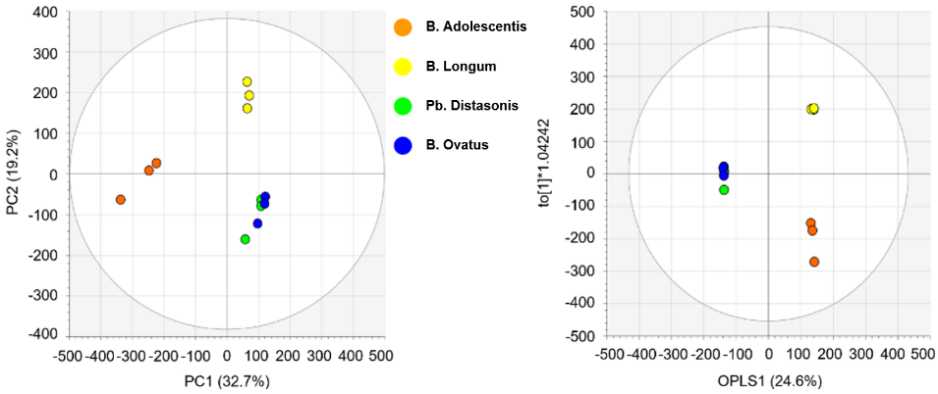

Supplementary Figures

Supplementary Figure 1A. Relative abundance of *Blautia obeum* between fecal samples from healthy controls and CRC patients

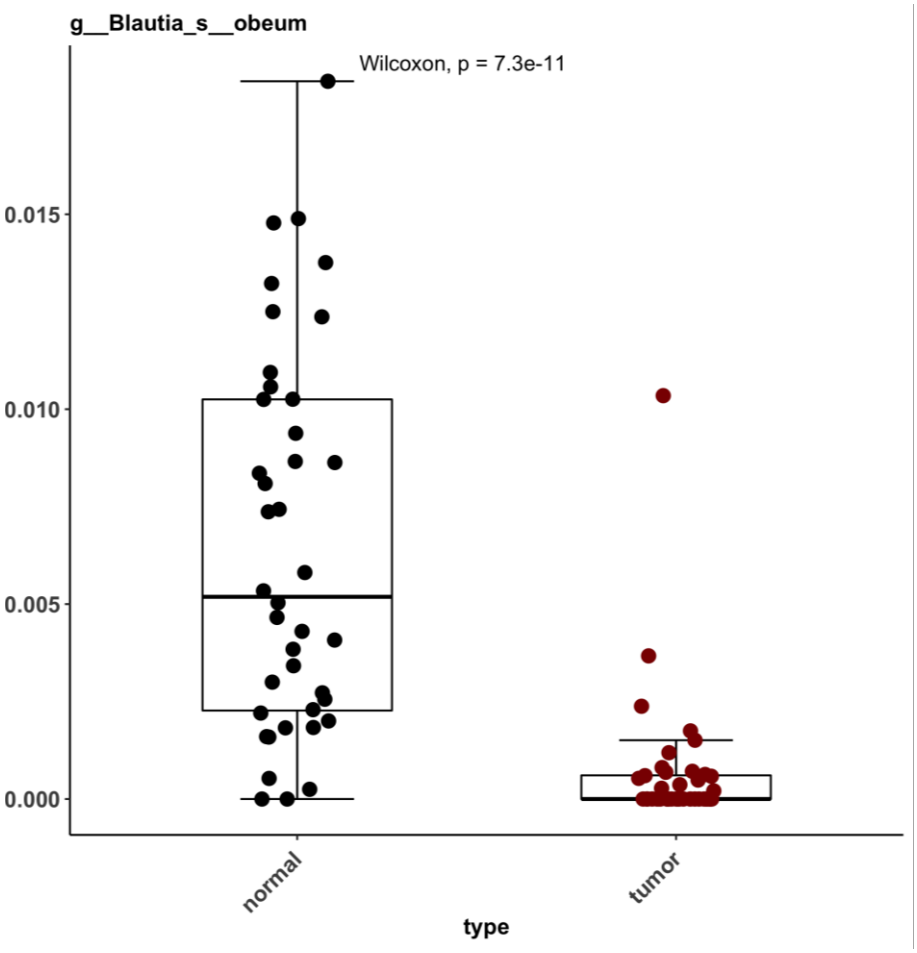

Supplementary Figure 1B. Relative abundance of *Blautia producta* between fecal samples from healthy controls and CRC patients

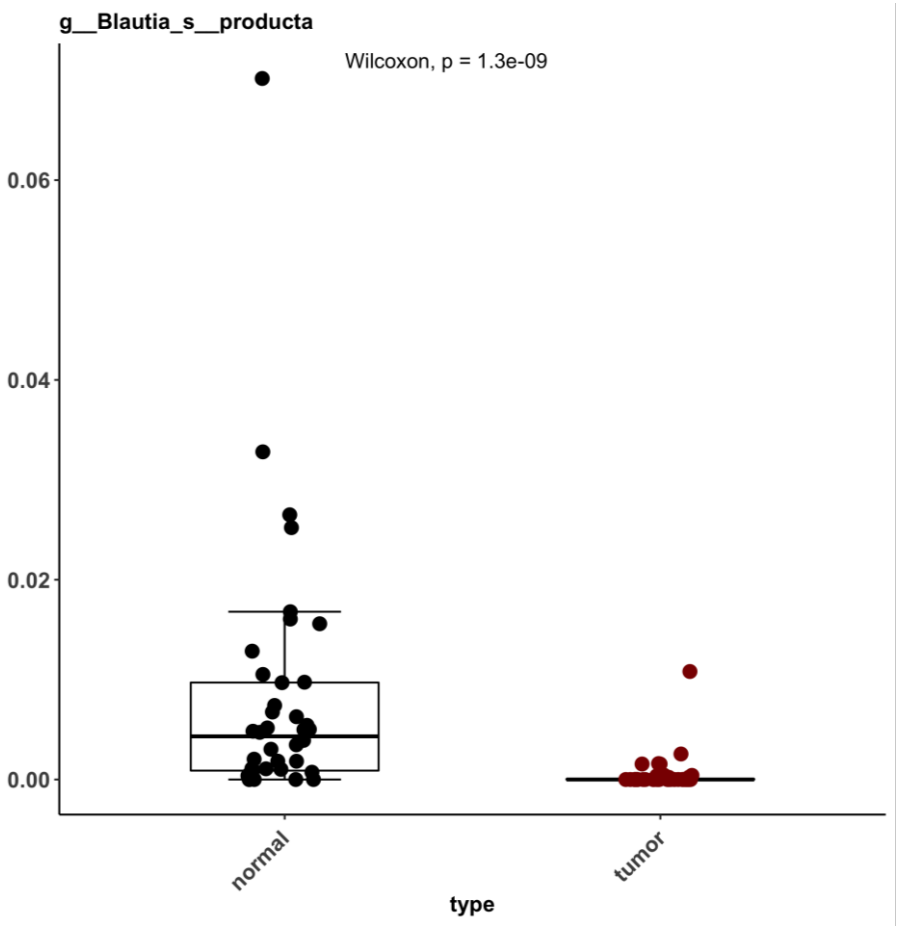

Supplementary Figure 1C. Relative abundance of *Dorea longicatena* between fecal samples from healthy controls and CRC patients

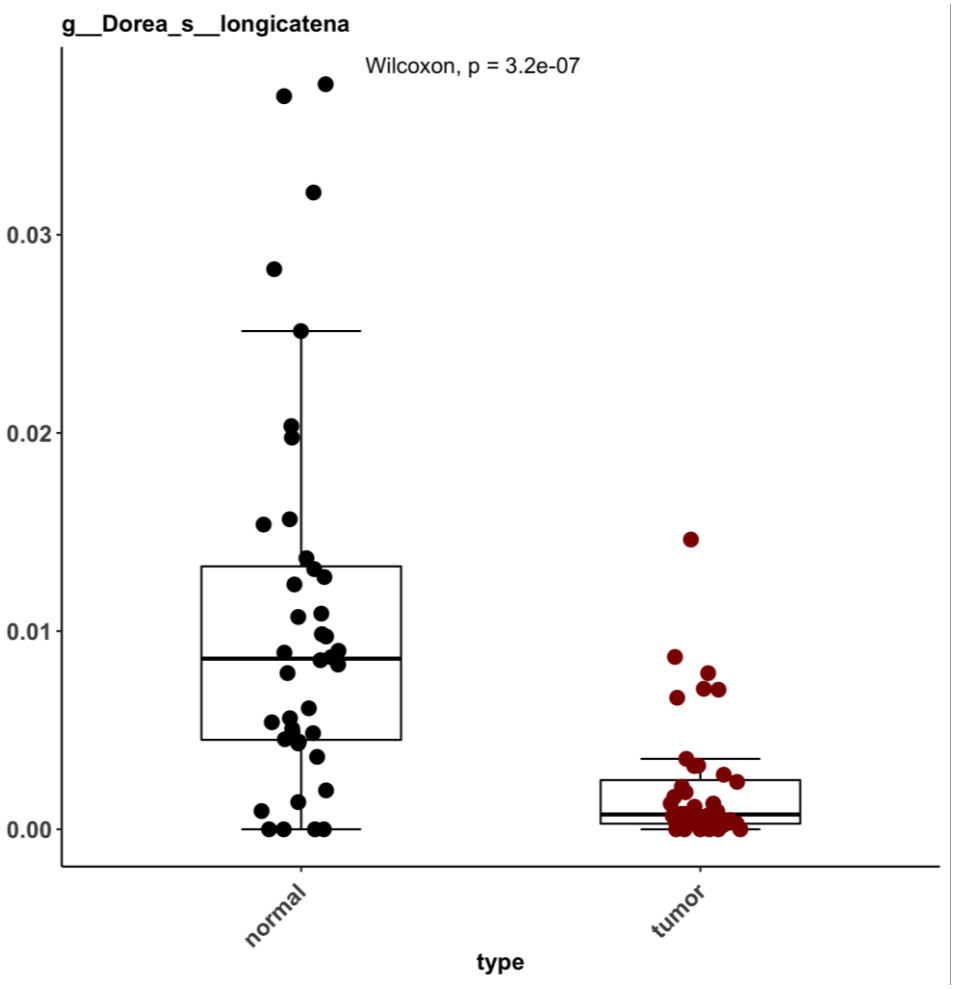

Supplementary Figure 1D. Relative abundance of *Faecalibacterium prausnitzii* between fecal samples from healthy controls and CRC patients

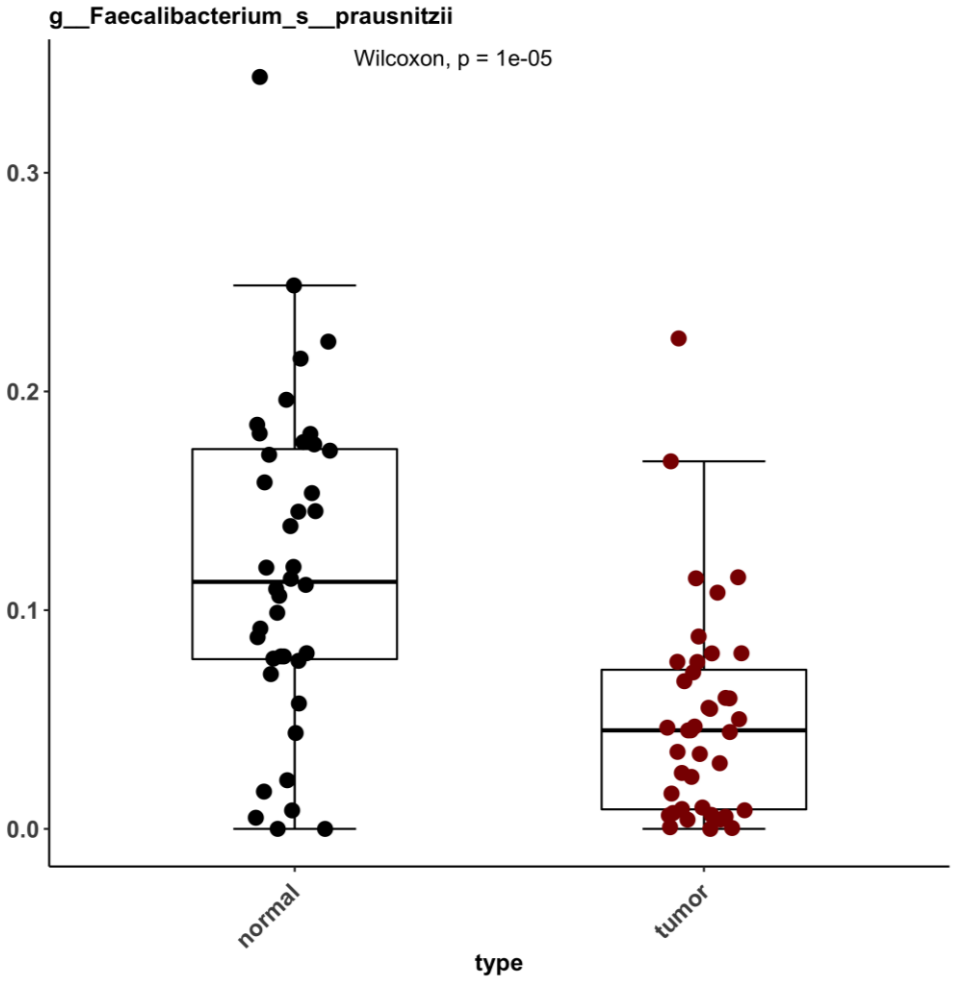

Supplementary Figure 1E. Relative abundance of *Clostridium celatum* between fecal samples from healthy controls and CRC patients

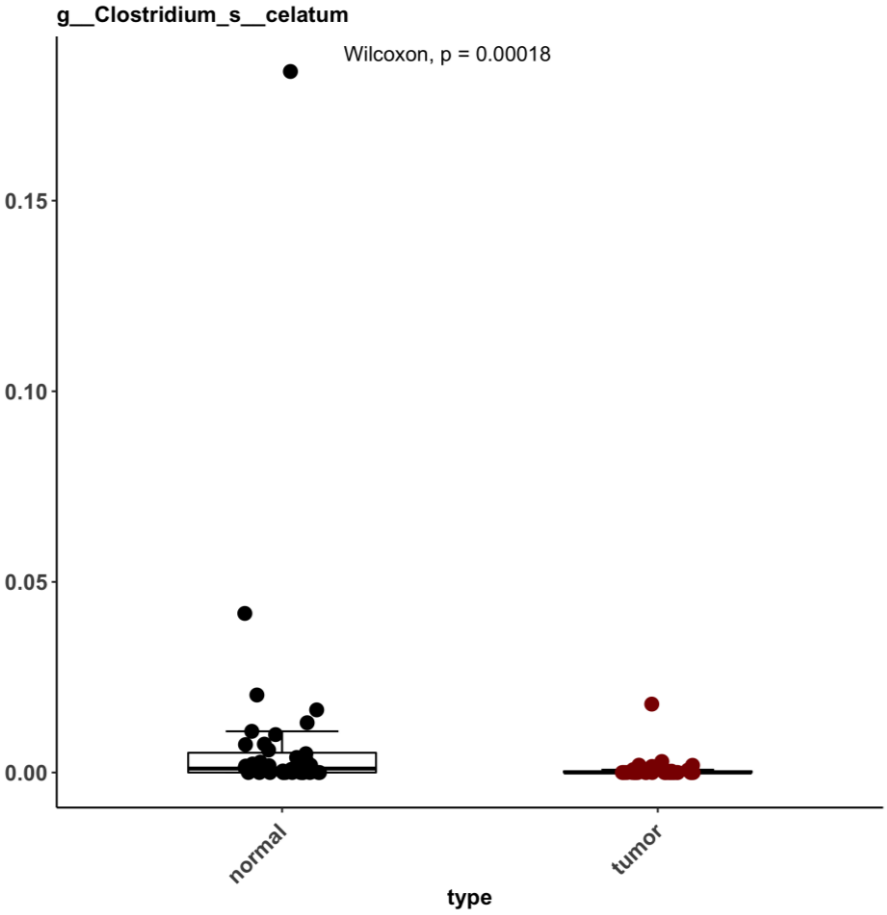

Supplementary Figure 1F. Relative abundance of *Bifidobacterium longum* between fecal samples from healthy controls and CRC patients

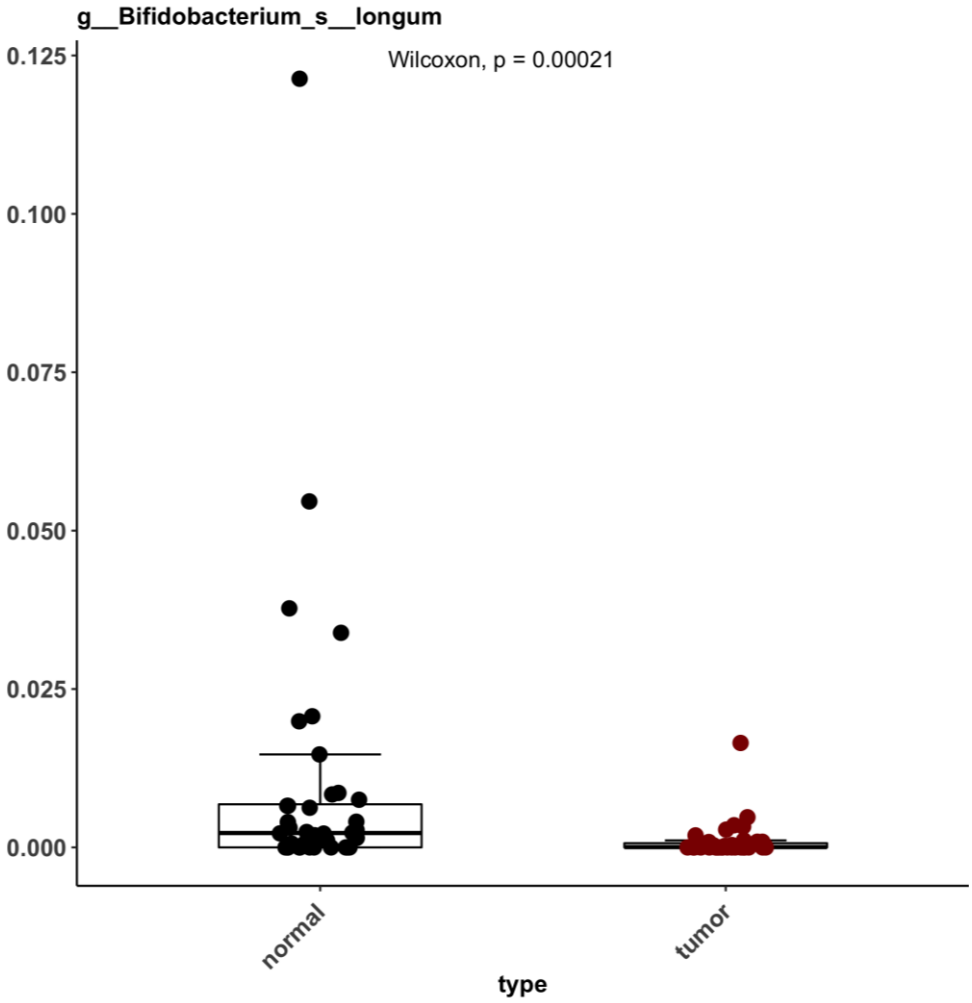

Supplementary Figure 1G. Relative abundance of *Bifidobacterium adolescentis* between fecal samples from healthy controls and CRC patients

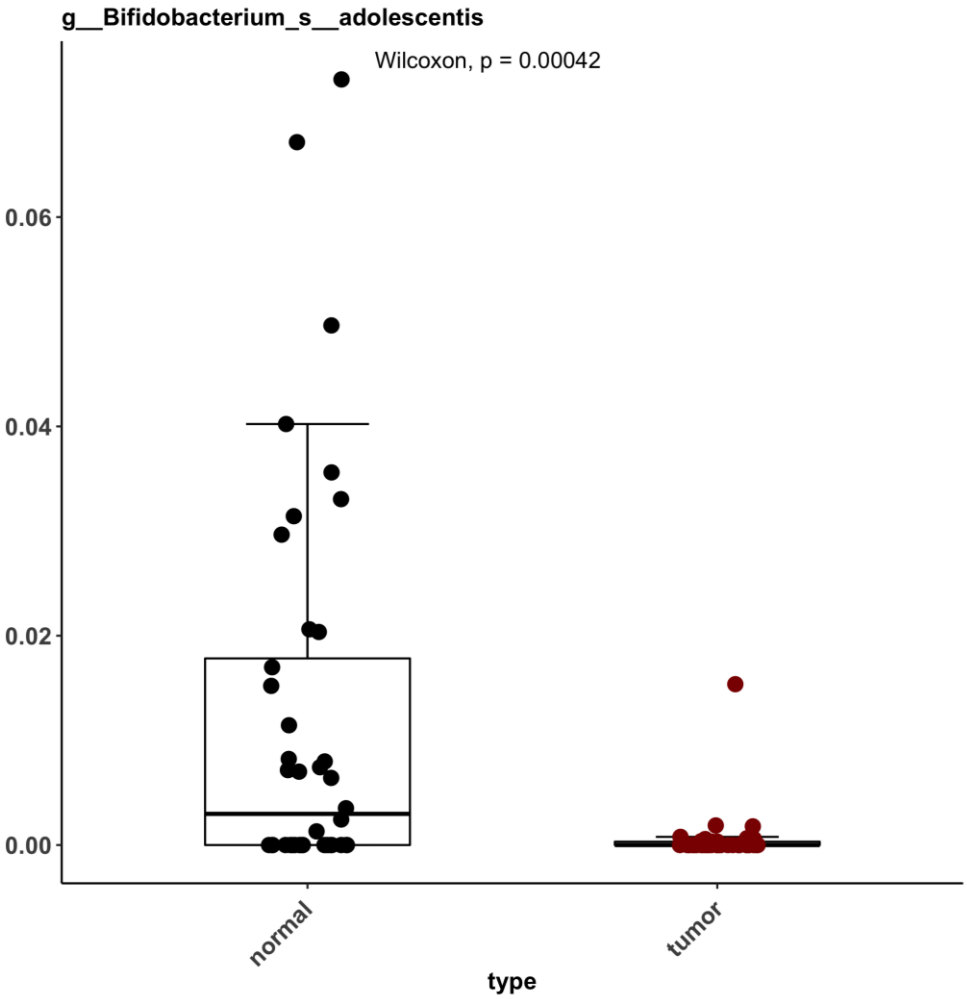

Supplementary Figure 1I. Relative abundance of *Lactobacillus ruminis* between fecal samples from healthy controls and CRC patients

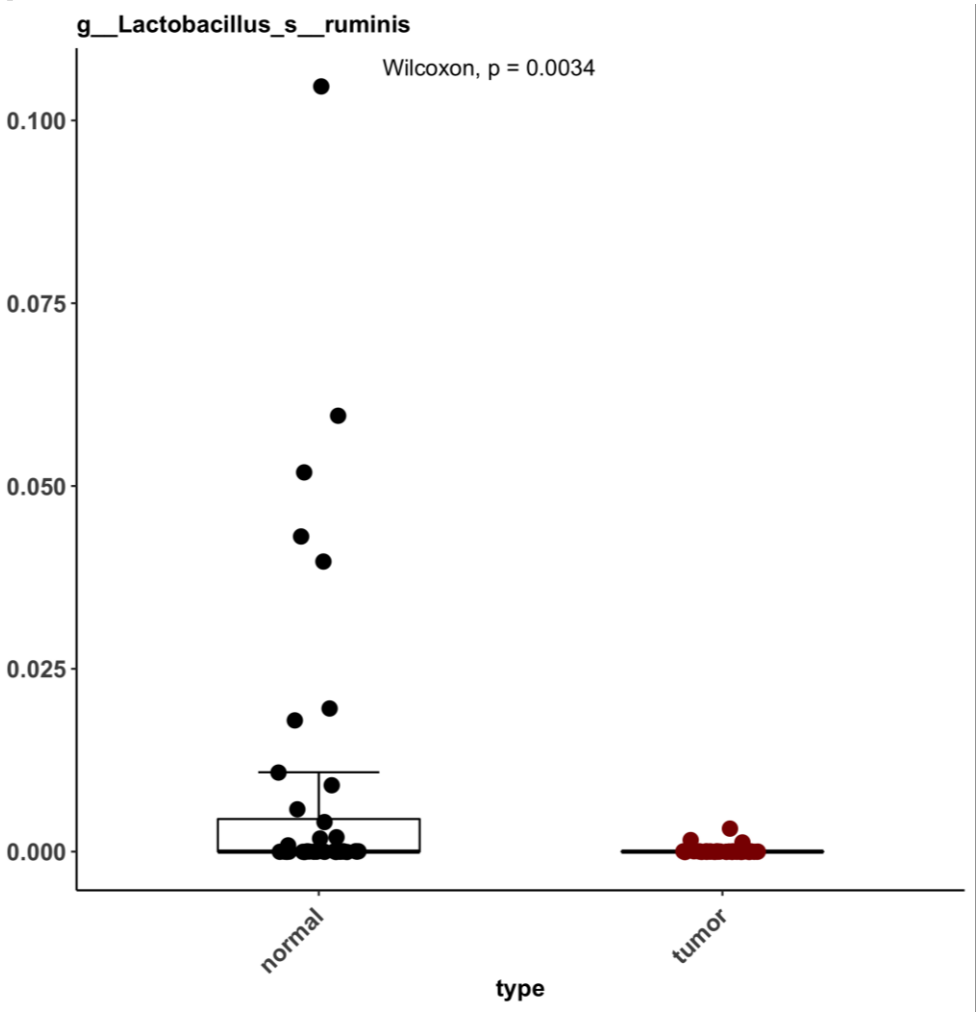

Supplementary Figure 1J. Relative abundance of *Ruminococcus callidus* between fecal samples from healthy controls and CRC patients

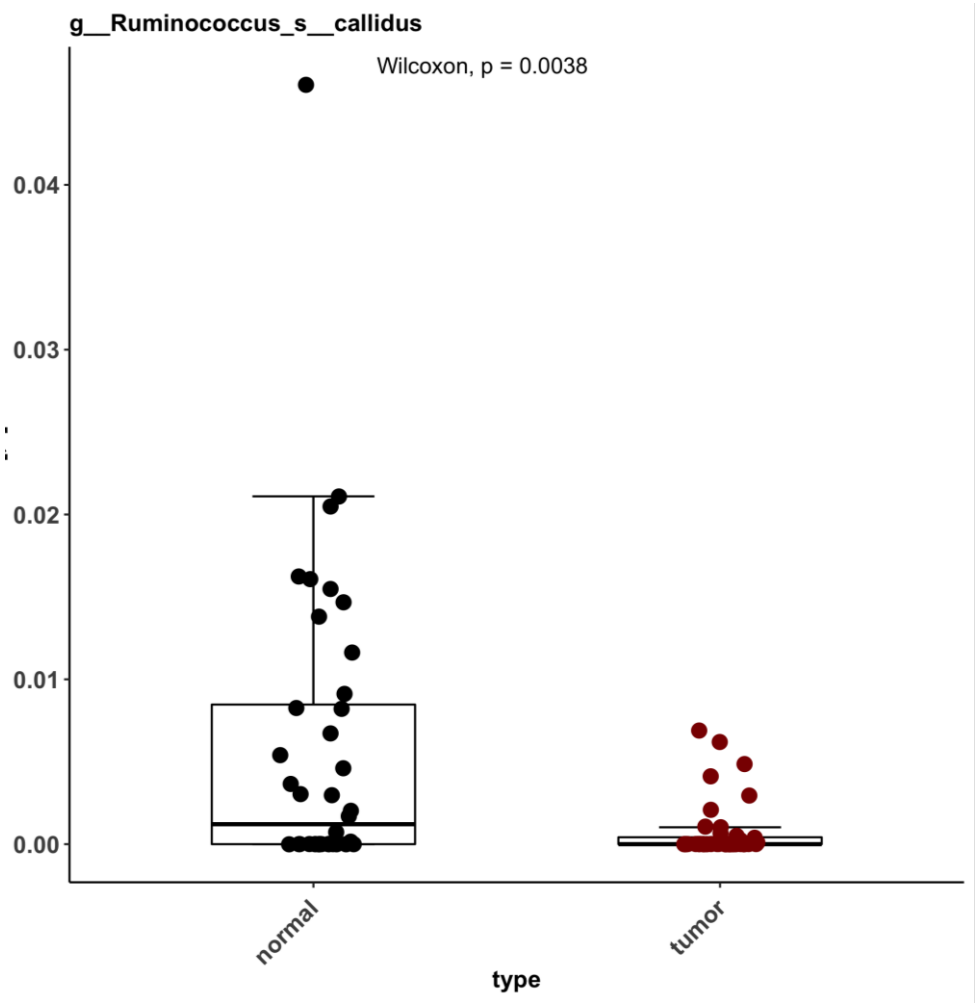

Supplementary Figure 2A. Relative abundance of *Prevotella stercorea* between fecal samples from healthy controls and CRC patients

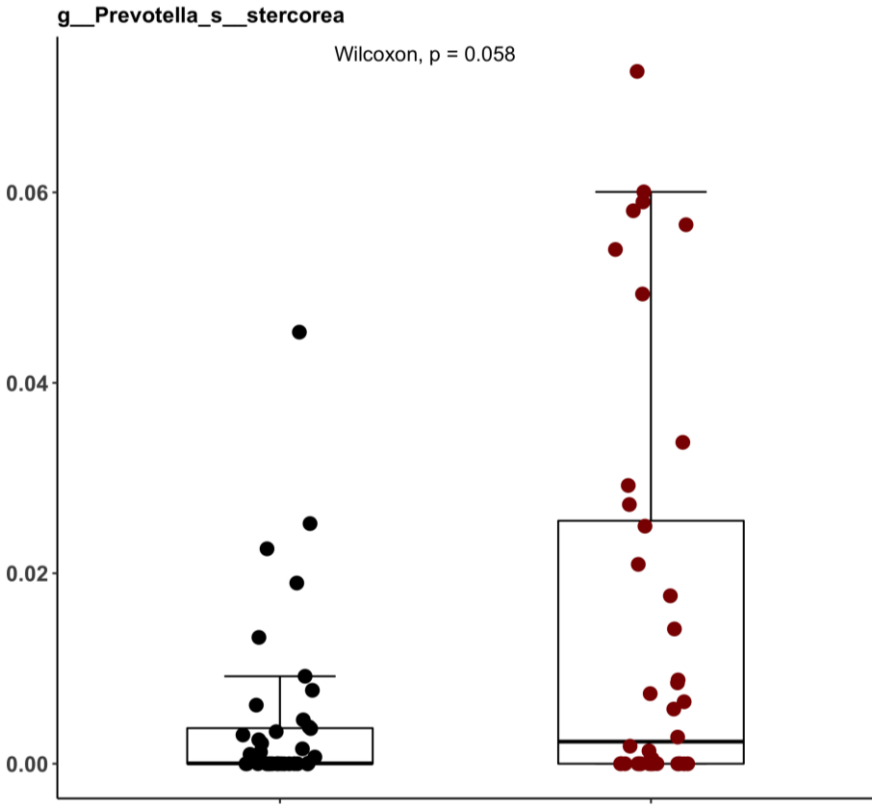

Supplementary Figure 2B. Relative abundance of *Parabacteroides distasonis* between fecal samples from healthy controls and CRC patients

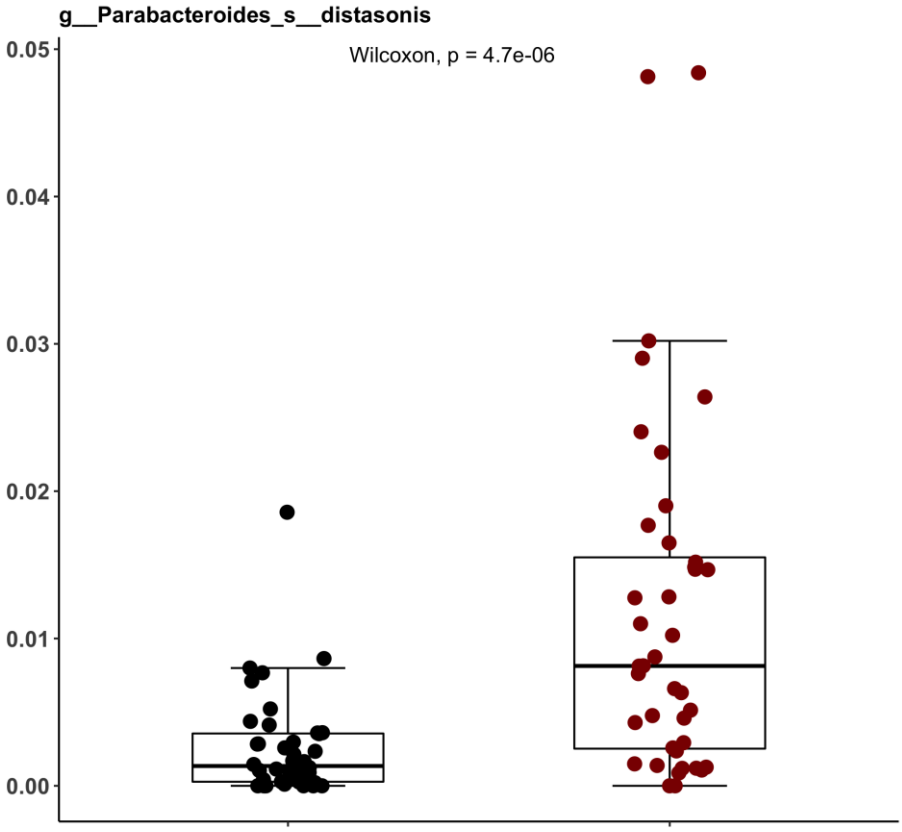

Supplementary Figure 2C. Relative abundance of *Bacteroides uniformis* between fecal samples from healthy controls and CRC patients

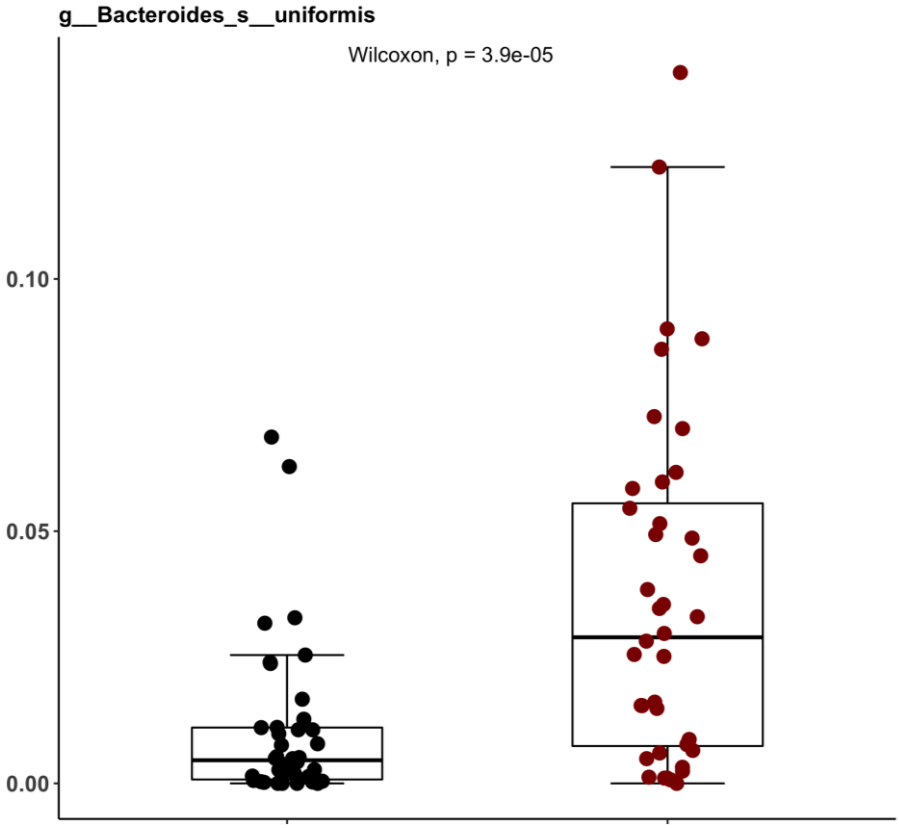

Supplementary Figure 2D. Relative abundance of *Bacteroides ovatus* between fecal samples from healthy controls and CRC patients

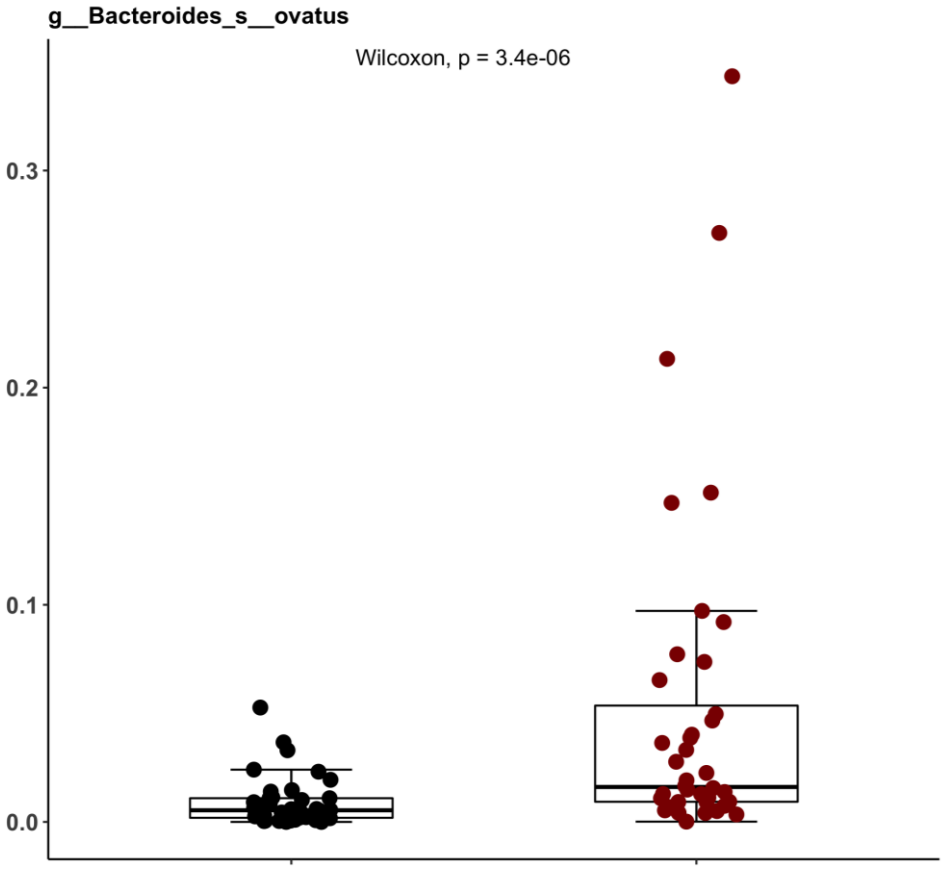

Supplementary Figure 2E. Relative abundance of *Bacteroides fragilis* between fecal samples from healthy controls and CRC patients

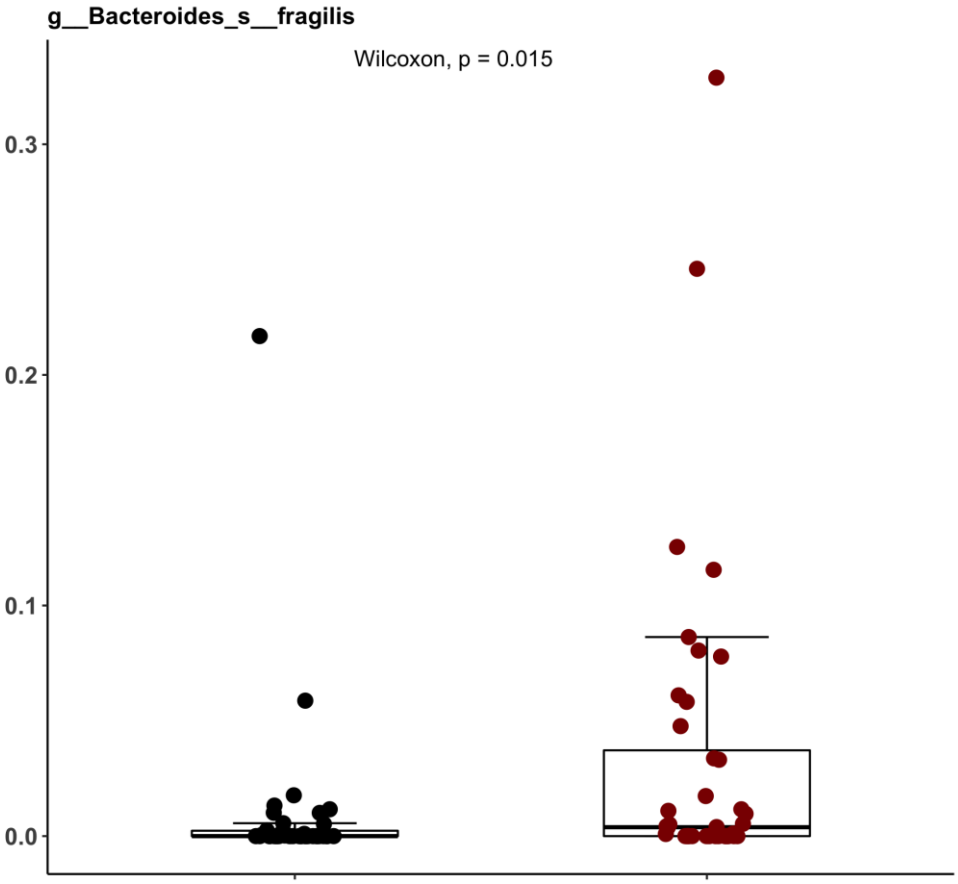

Supplementary Figure 2F. Relative abundance of *Bacteroides caccae* between fecal samples from healthy controls and CRC patients

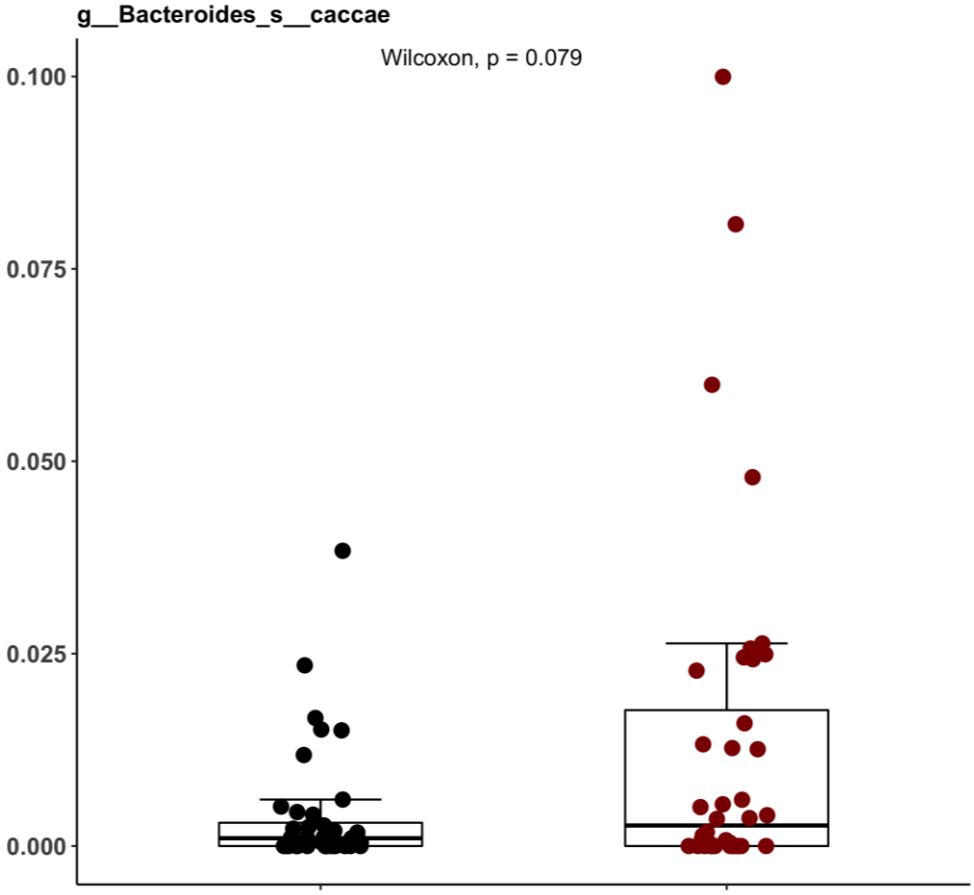

Abstract in Korean

장내 마이크로바이옴과 그 대사산물은 신진대사, 염증 및 면역 조절에 중추적 역할을 한다. 다양한 요인이 각 개인의 장내 마이크로바이옴 구성을 결정하는데, 그 중에는 유전적 소인, 출생 방법, 생활 방식, 질병 및 약물에 대한 노출이 미생물 구성을 결정하는 것으로 알려져 있다. 마이크로바이옴의 항상성 파괴된 상태, 즉 Dysbiosis 는 대장암의 종양 형성 및 진행에 관여하는 것으로 보고되어 왔다. 그러나 박테리아 분비 대사 산물(metabolome)이 대장암의 진행에 어떻게 영향을 미치는지는 아직 밝혀지지 않았다. 본 연구에서는 16S rRNA 분석을 통해 대장암 환자 분변의 미생물 구성을 건강한 대조군 분변과 비교하여 대장암 환자에서 미생물 구성에 차이가 있음을 확인하였고, 이는 기존 연구들과 유사한 결과를 보였다. 이에 대장암 환자의 분변에서 풍부한 마이크로바이옴 2종과 건강인의 분변에서 풍부한 마이크로바이옴 3종을 선정하여 각 미생물 배양액의 상층액을 대장 상피 오가노이드 및 대장암 오가노이드에 처리하여 오가노이드 성장을 비교 분석하였다. 그 결과, 건강인의 분변에서 풍부한 마이크로바이옴인 *Blautia producta*, *Bifidobacterium adolescentis*, and *Bifidobacterium longum* 에서 유래한 대사물이 대장암 오가노이드 성장을 유의미하게 저해하는 것을 확인하였고, 그 대사물의 주된 성분 차이가 butyric acid 에 있음을 확인하였다. 이후 RNA 분석 및 pathway 분석을 통해 Bifidobacterium 2 종에서 유래한 대사물이 대장암 성장 억제 효과가 있을 수 있다는 것을 확인하였다.